

Electronic Theses and Dissertations, 2004-2019

2019

Design of Unimorph Out-of-Plane Piezoelectric Actuator

Kevin Chan
University of Central Florida

 Part of the [Power and Energy Commons](#)
Find similar works at: <https://stars.library.ucf.edu/etd>
University of Central Florida Libraries <http://library.ucf.edu>

This Masters Thesis (Open Access) is brought to you for free and open access by STARS. It has been accepted for inclusion in Electronic Theses and Dissertations, 2004-2019 by an authorized administrator of STARS. For more information, please contact STARS@ucf.edu.

STARS Citation

Chan, Kevin, "Design of Unimorph Out-of-Plane Piezoelectric Actuator" (2019). *Electronic Theses and Dissertations, 2004-2019*. 6825.
<https://stars.library.ucf.edu/etd/6825>

DESIGN OF
UNIMORPH OUT-OF-PLANE PIEZOELECTRIC ACTUATOR

by

KEVIN CHAN
S.B. Harvard University, 2006

A thesis submitted in partial fulfillment of the requirements
for the degree of Master of Science
in the Department of Electric and Computer Engineering
in the College of Engineering and Computer Science
at the University of Central Florida
Orlando, Florida

Summer Term
2019

© 2019 Kevin Chan

ABSTRACT

Electromechanical transduction is an important component of microelectromechanical systems (MEMS), a technology with wide-ranging applications, including mobile computing, sensors, energy harvesting, and displays. These disparate applications have varying performance requirements, but generally transduction efficiency, mechanical precision, response time, cost, compatibility with photolithography and other fabrication processes, and operability at micro-scale are all desired metrics for MEMS devices. Piezoelectric transduction provides substantial advantages, including precise displacements, quick response times, and high transduction efficiency. These strengths make piezoelectric transduction particularly well-suited for use in resonators, sensors, and energy harvesters. However, piezoelectric transduction also produces much smaller magnitudes of movements than other electromechanical transduction mechanisms, such as thermal or capacitive. This limits the utility of piezoelectricity in designing MEMS actuators. Currently, MEMS designers compensate for this limitation by using sophisticated structures to amplify the small strains produced through the reverse piezoelectric effect. One of the oldest and simplest such designs is the bimorph cantilever beam. Comprised of two distinct, but mechanically connected, piezoelectric layers, the beam uses piezoelectricity to cause longitudinal strain in both layers. As one layer expands, the other contracts—this opposing motion creates a bending moment, causing the beam to deflect out-of-plane, often at substantially higher displacements than the expansion or contraction of either piezoelectric layer. This thesis presents a design and simulation results for a unimorph beam comprised of only one piezoelectric layer. Through use of a novel electrode pattern that applies a non-uniform electric

field, this beam acts as a quasi-bimorph, creating a bending moment without the need for two distinct piezoelectric layers.

This is dedicated to my parents, who have always pushed me to maximize my magnitude while letting me pick my own direction, and to the friends and colleagues who showed me that few things that are worthwhile can be achieved working in isolation.

ACKNOWLEDGMENTS

The research and design presented in this thesis was conducted in fulfillment of a research partnership between Truventic, LLC and the Dynamic Machine Lab of Dr. Reza Abdolvand at UCF. Partial funding for this research came through a contract between Truventic, LLC and the Department of Defense (U.S. Air Force.)

All finite element simulation (FES) data and plots were generated using COMSOL multi-physics simulation software, under a research license with UCF.

TABLE OF CONTENTS

LIST OF FIGURES	ix
CHAPTER ONE: INTRODUCTION.....	1
Overview of MEMS.....	1
Background.....	3
CHAPTER TWO: PIEZOELECTRIC TRANSDUCTION.....	9
Piezoelectric Materials.....	9
Modeling Piezoelectricity	11
Material Orientation.....	16
Device Fabrication	17
CHAPTER THREE: BIMORPH BENDING BEAMS	20
Structure of Bimorph Beam.....	20
Electric Field Pattern.....	22
CHAPTER FOUR: NOVEL ELECTRODE PATTERN.....	26
Advantages of a Unimorph Design.....	26
Operation of Novel Electrode Pattern.....	27
CHAPTER FIVE: LITHIUM NIOBATE.....	36
Selection of Lithium Niobate.....	36
Rotated Piezoelectric Strain Coefficients	37

CHAPTER SIX: UNIMORPH BEAM DESIGN	43
Torsion Actuation	43
Bending Actuation	45
Electrode Pattern Revision.....	49
Multistage Actuator	54
CHAPTER SEVEN: RESULTS AND CONCLUSIONS	63
Results.....	63
Comparison to Published Works	63
Conclusions.....	71
LIST OF REFERENCES	73

LIST OF FIGURES

Figure 1. Layer composition of RF switching beam.....	4
Figure 2. Overhead diagram of folded bimorph actuator.	6
Figure 3. Diagram of cross section of crystal lattice with inversion symmetry.	10
Figure 4. Infinitesimal cube representing Cauchy point stress.	12
Figure 5. Positive strain resulting from stress pulling apart Face 2 and its opposite face.	13
Figure 6. Strain resulting from shear stress.	14
Figure 7. Axis orientation with respect to substrate wafer orientation (left) and with respect to MEMS beam orientation (right).....	18
Figure 8. Diagram of simple bimorph beam.....	20
Figure 9. Unequal strain develops bending moment.	21
Figure 10. Cross sectional area of bimorph beam in larger structure.	22
Figure 11. Displacement plot of bimorph aluminum nitride beam.....	24
Figure 12. COMSOL model of individual aluminum nitride beams.....	25
Figure 13. Top view of signal electrodes for SAW device.....	28
Figure 14. Electric field pattern along longitudinal cross-section of surface acoustic wave (SAW) pattern beam.....	29
Figure 15. Plot of longitudinal (axis 1) component of electric field along length of SAW beam.....	29
Figure 16. Plot of z-axis (axis 3) component of electric field along length of SAW beam.....	30
Figure 17. Electric field arrow plot along lateral cross-section of beam with laterally placed electrodes.	31

Figure 18. Plot of electric field lines on lateral cross-section of beam with top and bottom twin electrodes.	33
Figure 19. Arrow plot of electric field on lateral cross-section of beam with top and bottom twin electrodes.	34
Figure 20. COMSOL model of unimorph beams at varying orientations within the x-cut plane. (Rotated coordinate system used for piezoelectric model.)	40
Figure 21. Parametric sweep of the total deflection of a test structure rotated about the x-axis. .	41
Figure 22. Model of test structure in x-cut lithium niobate, displaying bending and twisting components.	42
Figure 23. Model of torsion beam actuator with perpendicular cantilever beam.	44
Figure 24. Unimorph bending actuator.	45
Figure 25. Initial bending multistage actuator design.	46
Figure 26. Model of bending beam with reversal of polarity.	48
Figure 27. Multistage bending beam actuator with reversals.	48
Figure 28. Streamline plot of electric field along lateral cross-section of unimorph beam. (Dual top electrodes: signal and ground. Single bottom electrode: ground.)	50
Figure 29. Displacement plot of single ground beam.	51
Figure 30. Revised electrode pattern with single top electrode, continuous bottom ground.	52
Figure 31. Streamline plot of unimorph beam with single top signal electrode and continuous bottom ground electrode.	53
Figure 32. Multiple bending beams in stages provide greater total displacements.	55

Figure 33. Parametric plot of vertical deflection of a single, 100 micrometer unimorph beam as a function of beam width.	57
Figure 34. Layout of spiral actuator design.	59
Figure 35. Simplified and scaled layout of spiral design to show top electrode pattern.	60
Figure 36. Simulation of spiral actuator design.	62
Figure 37. Simulation of 200 micrometer cantilever beam.	64
Figure 38. COMSOL simulation of bimorph modeled by Kawakubo et al.	65
Figure 39. Simulation of half-micrometer thick unimorph beam.	66
Figure 40. Folded capacitor tuning actuator using unimorph beam components (1 micrometer thick).	67
Figure 41. Folded capacitor tuning actuator using dual-polarity unimorph beam components (1 micrometer thick).	69
Figure 42. COMSOL simulation of 1000 micrometer unimorph beam.	71

CHAPTER ONE: INTRODUCTION

Overview of MEMS

Microelectromechanical systems (MEMS) are the technology of designing, manufacturing, and operating devices with components that are micrometer-scale in size. The term was first used in a DARPA proposal in the 1980's; however, the field itself is somewhat older, with MEMS strain sensors being demonstrated over a decade earlier. For a long time, MEMS devices were largely limited to research, failing to demonstrate advantages over analogous, macro-scale technology. However, this has since changed drastically, due in large part to the demand-driven development of electronics and computing. The reason for this is twofold. First, the demand for better, faster, and smaller electronics has driven research in many fields related to integrated chip design, including semiconductor materials research and photolithography. These advancements are readily applied to microfabrication of MEMS devices, facilitating the advancement of MEMS research. Second, the advancement of electronics to the point where electronic devices can be so small, powerful, and mobile that the traditional, macro-scale electromechanical components are the limiting factor. This has driven demand for electromechanical components that can be scaled down similarly. Today, MEMS devices are found in a wide variety of applications, most often as a component of a more complex device.

From the use of the term “electromechanical” in its name, it is no surprise that electromechanical transduction—the conversion of energy from the electrical domain to the mechanical domain, and vice versa—is integral to the operation of MEMS devices. Several

mechanisms are widely used not only in MEMS, but also in larger scale devices. Each has distinct advantages and disadvantages. Thermal actuation uses resistive heating to convert an electrical signal to thermal energy, which in turn transduces into the mechanical domain through thermal expansion. This mechanism has some uses in smaller devices, but at larger scale its response time is limited by the rate of passive cooling. Electrostatic actuation uses the electrostatic force to drive movement. Magnetic actuation generates an electromagnetic field to drive mechanical movement. It has the advantage of producing strong forces and large displacements; however, it also suffers from high energy consumption and process compatibility issues with microfabrication.

Piezoelectric transduction relies on a unique material property to couple the electric and mechanical domains directly. Due to an asymmetry in the charge distribution of their crystal lattice structures, piezoelectric materials produce strain (physically deform) in response to an applied electric field and likewise develop an electric charge in response to applied mechanical stress. Piezoelectricity has many useful properties for MEMS devices. It provides efficient transduction, allowing piezoelectric devices to operate with high efficiency and generally giving piezoelectric resonators superior quality factor Q . Because piezoelectric behavior arises from a property of the smallest crystal unit cell of a material, piezoelectric structures can be scaled down substantially and maintain its piezoelectric properties, and piezoelectric materials are more generally compatible with MEMS fabrication processes. Piezoelectric transduction produces small strains in response to comparatively large electric fields—this allows piezoelectric actuators to achieve very precise control over mechanical movements. However, this property is

always piezoelectric transduction's greatest limitation—it cannot readily produce the larger displacements of other transduction mechanisms.

Currently, MEMS designers partially compensate for this limitation by creating compound piezoelectric devices to improve the displacements yielded by piezoelectric devices. One of the earliest and simplest solutions is the bimorph cantilever beam. The bimorph MEMS device comprises two separate piezoelectric layers and several electrically conductive layers. Different electrical signals are applied to each layer, inducing a different electric field in each layer.

This results in one layer contracting horizontally (within the plane of the device), while the other layer expands along the same axis. These opposing strains result in a bending moment, causing the beam to bend vertically (out of the plane of the device.) This out-of-plane displacement can be substantially greater than the in-plane motion of either layer, increasing the utility of the piezoelectric structure as a MEMS actuator; however, this more complicated structure increases the number of photolithography steps required for fabrication, resulting in increased cost, more complicated processing, greater manufacturing times, and more opportunities for contamination or damage during fabrication.

Background

As previously discussed, MEMS devices offer numerous advantages over existing solutions to different technical challenges. In the field of RF switching, MEMS switches offer lower power consumption, improved isolation, and superior isolation in comparison to existing solutions such as FET and diode switches. [1] One paper presented a low voltage, cantilever MEMS device for RF switching. Though it described the design as a “unimorph” piezoelectric

beam, the composition of beam is in fact closer to a classic bimorph beam. The beam consists of two separate aluminum nitride layers and three conducting layers, two thin platinum layers and one thicker gold layer. The study presents this as a unimorph design because only one piezoelectric layer is an “active layer”—that is, the two platinum layers in contact with that layer apply a controlled electric signal in order to trigger a specific piezoelectric response. The thick gold layer acts as the conductor for the switch, while the second aluminum nitride layer acts as an isolation layer between the RF signal and the switching signal.

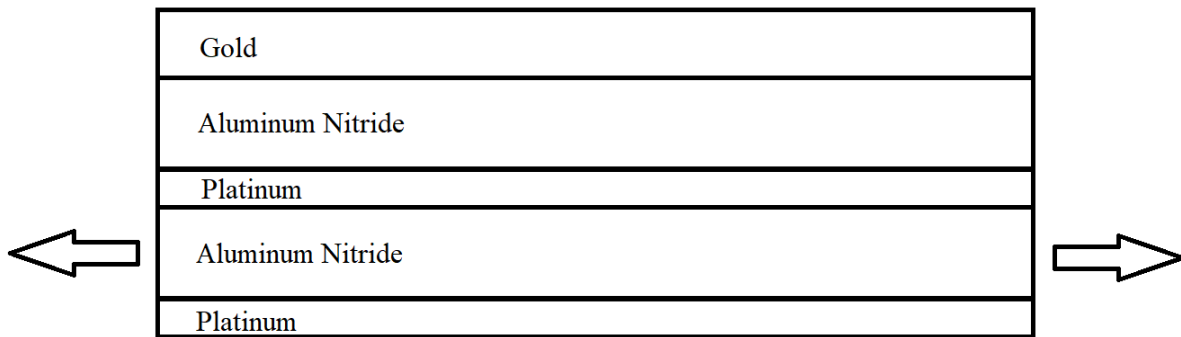


Figure 1. Layer composition of RF switching beam.

The design thus operates much like a classic bimorph, with the positive longitudinal strain of one piezoelectric layer acting against the zero strain of the other piezoelectric layer (as well as the thick gold layer.) This is not a true unimorph beam, as the action of the single active piezoelectric layer would not be able to produce a substantial bending moment without the stiffness of the “passive” layers. In fact, the study itself demonstrated the importance of these passive layers by modeling the effect of the gold layer thickness on beam deflection. A 200 micrometer long beam with micrometer-thick aluminum nitride layers can achieve deflections ranging from less than 100 nanometers to roughly 650 nanometers, depending entirely on the thickness of the gold layer.[1]

Tunable capacitors present another application requiring MEMS actuators capable of producing large but precise displacements. The capacitance of a parallel plate capacitor depends in part on the separation of the two conducting plates. One paper presents a design using a folded bimorph actuator move one of the plates in the capacitor, modifying the separation distance and thus the capacitance of the device. [2] The basic component of their folded actuator is a bimorph cantilever beam comprised of three 200 nanometer thick aluminum layers and two 500 nanometer thick aluminum nitride layers. Using solid mechanics, the study calculated a deflection of roughly 1.3 micrometers for a 200 micrometer long beam and an actuation signal of 5 volts. Because the bending moment introduces a tilt at the distal end of the beam, the tunable capacitor utilized folded design that maintained the capacitor plate in a parallel orientation. The folded beam consists of one or two piezoelectric bimorph beams anchored to the substrate. At the distal ends, these beams connect to a moving structure that connects to a third bimorph beam. This structure curves upwards substantially, primarily due to stresses deliberately introduced to the piezoelectric layers during sputtering. The third bimorph beam, anchored to this structure, projects towards the original anchor point and actuates the capacitive plate at its distal end. [2]

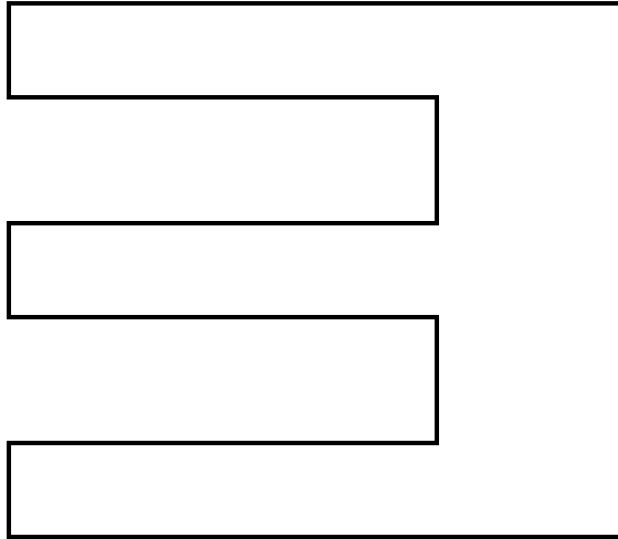


Figure 2. Overhead diagram of folded bimorph actuator.

The study presented results from physical prototypes using several variations of this design, some comprised of 200 micrometer bimorph beam components, others using 400 micrometer beams. The best result from the 200 micrometer designs yielded a deflection of slightly over 2 micrometers; the best 400 micrometer design yielded a deflection of nearly 8 micrometers. These designs were actuated with signals up to roughly 5.5 volts, and some required complex patterning of the bimorph layers with via holes to permit the proper signaling to the complex structure. [2]

Many designs use aluminum nitride due to process compatibility. Another material, lead zirconate titanate (PZT), has limited applicability due to the presence of lead, which in particular prevents its integration with CMOS processes. However, PZT does exhibit far superior piezoelectric properties, and PZT piezoelectric bimorph designs yield the highest deflections among the published works. One paper compared the performance of what it called PZT monomorph structures to its own bimorph design. [3] The monomorph structure consisted of a

single 350 nanometer layer of PZT between two 100 nanometer platinum layers. This stack was bonded to a 680 nanometer polysilicon layer; the stiffness of this layer creates the bending moment by resisting the piezoelectric contraction of the PZT layer. Using unspecified finite element simulation, the study claimed roughly 80 micrometer deflections for 1000 micrometer long PZT bimorph structures comprised of a single 350 nanometer active PZT layer. The study describes a new design as a bimorph, replacing the single PZT layer with two separate 175 nanometer PZT layers in between three 100 nanometer platinum thin films. However, it would be overly simplistic to categorize this structure as a simple bimorph. The device applies electric fields of the same polarity to both piezoelectric layers, resulting in both layers contracting. The difference in the strengths of the electric field nonetheless creates a difference in the amount of contraction, yielding a bending moment. However, it is the presence of the same polysilicon layer present in the so-called monomorph design that contributes substantially to the bending moment. According to simulations in the study, the innovative PZT actuator produces threefold deflection compared to a comparable PZT monomorph, yield 280 micrometer deflections in response to 10 volts applied to a 1000 micrometer beam. The study announced the successful fabrication of the innovative design, but had yet to measure actual deflection. [3]

This thesis proposes a novel design that can produce high magnitude, out-of-plane displacements using a single piezoelectric layer. An innovative electrode pattern induces a non-uniform electric field in the piezoelectric layer, resulting in longitudinal expansion near the bottom of the device and longitudinal contraction near the top of the device. This results in out-of-plane bending using only a single piezoelectric layer and no more than two conducting

electrode layers, substantially simplifying the fabrication process. By changing the orientation of the structure fabricated from the same piezoelectric layer, a torsional (twisting) response can be achieved, allowing increased versatility in device design. This paper also presents a comprehensive design for a piezoelectric actuator comprised of these elements.

CHAPTER TWO: PIEZOELECTRIC TRANSDUCTION

Piezoelectric Materials

In 1880, Pierre and Jacques Curie first discovered piezoelectricity in quartz. [1] This property allows a material to transform energy between the mechanical domain and the electrical domain without the need for any sophisticated structures. Generally, when a linear elastic material experiences mechanical stress—for example, when an external force is applied—that stress will result in deformation of the material, or strain. When a grain of piezoelectric material experiences stress, the resulting deformation causes a change in the electrical polarization of the material. This phenomenon is called the *direct piezoelectric effect* and acts as a mechanism to transduce applied mechanical forces into an electrical response. This mechanism is reversible, meaning that the application of an electric field to a piezoelectric material likewise will cause that material to experience stress; this is known as the *converse piezoelectric effect* or *reverse piezoelectric effect*. [5]

Appropriately, quartz clocks were among the first commercial applications for piezoelectricity, taking advantage of the piezoelectric properties of quartz crystals to produce a stable frequency response that could be used in place of complex mechanical movements for timing. Today, more sophisticated crystal oscillators made from quartz or other materials remain widely used in research and practical applications. However, MEMS oscillators have begun to supplant bulk crystal and ceramic piezoelectric oscillators in many applications, offering several advantages at the cost of certain tradeoffs. In particular, the miniature scale of MEMS devices allows them to be more readily packaged with microelectronics, and there is substantial interest

in integrating MEMS devices and integrated chips within a single streamlined fabrication process. [6]. Piezoelectric MEMS oscillators, in particular, can be considered the next step in a process of evolution that began with the Curie brothers' discovery.

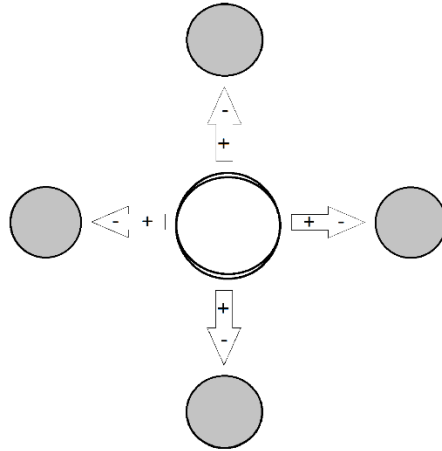


Figure 3. Diagram of cross section of crystal lattice with inversion symmetry.

Piezoelectricity arises in crystalline materials lacking inversion symmetry—that is to say, materials where each crystal unit cell has a center of symmetry in three dimensions. In a structure with inversion symmetry, if that center of symmetry is denoted $(0,0,0)$ in a Cartesian coordinate system, then every point (x,y,z) will be identical to point $(-x,-y,-z)$. Crystalline solids are held together by the chemical bonds between neighboring atoms. Atoms form these bonds by sharing or exchanging electrons; the atoms are then held together by the electrostatic attraction among their positively charged nuclei and the negatively charged shared electrons. Each bond can then form a dipole due to the asymmetrical distribution of charge. When a crystal unit cell has inversion symmetry, every bond corresponds to an identical bond, equal in magnitude but opposite in orientation and position. As a result, the dipoles within the cell cancel out, and the cell as a whole exhibits no measurable dipole when at electrostatic equilibrium.

In a piezoelectric material, the equilibrium charge distribution within each unit crystal cell is non-uniform due to the lack of inversion symmetry, resulting in a distinct dipole. The axis of the dipole is often referred to as the poling direction; piezoelectricity can be induced in some crystals or ceramics through a process called poling, in which inversion symmetry is destroyed by shifting the position of atoms in the lattice by applying a strong electric field. When the crystal structure deforms in response to stress, the positions of the atoms shift, resulting in a change in the electric field of the structure. When many of these individual crystal unit cells share the same orientation, the sum of their response can be observed in the bulk structure of the material. [7]

Modeling Piezoelectricity

Piezoelectric materials, like other linear elastic materials, obey Hooke's law, meaning that there is a linear relationship between stress and strain. Within the range of operating conditions the piezoelectric effect is also linear, meaning that the piezoelectric behavior of a system can be modeled using a set of linear equations. [5]

The electric field is expressed as a three-dimensional vector:

$$E = \begin{bmatrix} E_1 \\ E_2 \\ E_2 \end{bmatrix} \quad (1)$$

Stress is a measurement of the internal forces acting within an object. Stress is expressed as a second-order tensor, appropriately known as the Cauchy stress tensor:

$$\sigma = \begin{bmatrix} \sigma_{1,1} & \sigma_{1,2} & \sigma_{1,3} \\ \sigma_{2,1} & \sigma_{2,2} & \sigma_{2,3} \\ \sigma_{3,1} & \sigma_{3,2} & \sigma_{3,3} \end{bmatrix} \quad (2)$$

To understand the stress tensor, it is helpful to visually each point within a material as an infinitesimally small cube. Any stress experienced by that cube can be expressed as a sum of

individual components of force acting upon that cube; in turn, each of those components can be described in terms of three perpendicular surfaces of the cube. For an infinitesimally small cube, the force acting on one face will be equal in magnitude to the force acting on the opposing face—thus, the value of the forces acting upon only three perpendicular faces form a complete description of the total force acting upon the system.

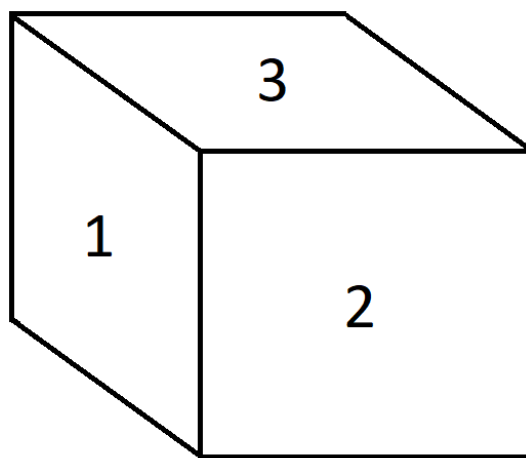


Figure 4. Infinitesimal cube representing Cauchy point stress.

The normal components ($\sigma_{1,1}$, $\sigma_{2,2}$, and $\sigma_{3,3}$) describe stress resulting from force acting on one face and its opposite. These are the stress components that cause a material to expand or contract along an orthogonal direction. In this example $\sigma_{1,1}$ would be the stress pushing Face 1 and its opposite face together (negative stress) or pulling them apart (positive stress.) The first subscript denotes the face the force acts upon, while the second subscript indicates the direction of the force. Thus, each component with two identical subscripts reflects force normal to the face affected. Because the cube does not accelerate, a force equal in magnitude and opposite in direction must affect the opposite face.

This stress component, acting on its own, would tend to cause square Face 2 and Face 3 to become non-square rectangles as the material expands or constricts. Normal stress along any axis can be expressed as a sum of normal stress components along any three orthogonal axes—for example, the x, y, and z axes in a Cartesian coordinate system.

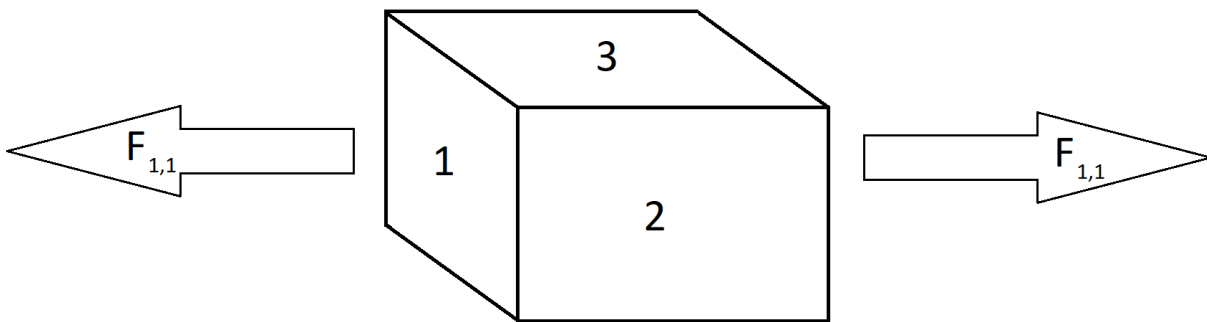


Figure 5. Positive strain resulting from stress pulling apart Face 2 and its opposite face.

However, the net normal stress on this cube does not fully describe the total stress at this point—it is also necessary to account for shearing stress. While normal stress can be conceptualized in terms of perpendicular forces acting on each face in the cube, shear stress is the result of forces that are tangential to the face being affected. Consider stress component $\sigma_{3,1}$. The first subscript denotes the faces affected by the forces: Face 3 and its opposite face. The second subscript indicates the direction of the force—in this case, in the direction normal to Face 1. The force on the opposite face must be equal in magnitude and opposite in direction in order to have net zero force on the cube. As a result, this stress component tends to move Face 3 away from its opposite, but in a direction within the plane of the face. The following figure illustrates the strain response to shear stress.

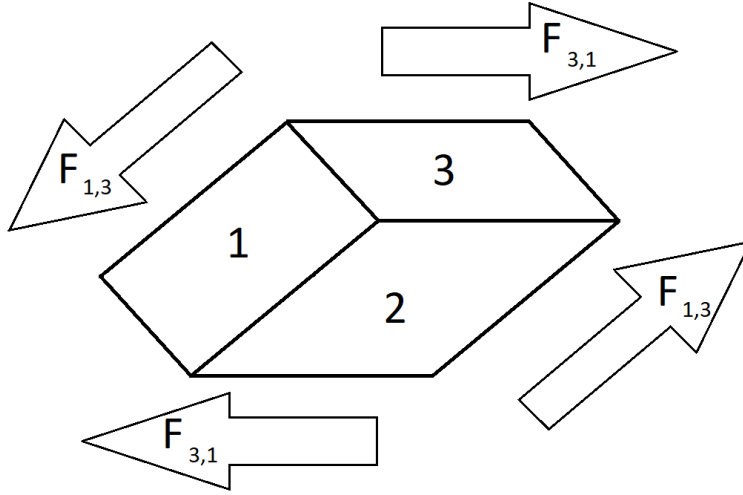


Figure 6. Strain resulting from shear stress.

Due to the symmetry of the shear stress components, the magnitude of any component $\sigma_{n,m}$ will be equal to the magnitude of any component $\sigma_{m,n}$. This means that only three shear stress components are necessary to convey the total shear stress acting upon the cube. Thus, it is possible to reduce the full nine elements of the Cauchy stress tensor to a six-dimensional vector without any loss of information. Strain, the deformation of a material in response to stress, is also expressed as a second order tensor, and thus can similarly be expressed as a six-dimensional vector.

$$\sigma = \begin{bmatrix} \sigma_{1,1} & \sigma_{1,2} & \sigma_{1,3} \\ \sigma_{2,1} & \sigma_{2,2} & \sigma_{2,3} \\ \sigma_{3,1} & \sigma_{3,2} & \sigma_{3,3} \end{bmatrix} \xrightarrow{\text{yields}} \begin{bmatrix} \sigma_{1,1} \\ \sigma_{2,2} \\ \sigma_{3,3} \\ \sigma_{2,3} \\ \sigma_{3,1} \\ \sigma_{1,2} \end{bmatrix} \quad (3)$$

This allows the electromechanical coupling of a piezoelectric material to be fully described in terms of a system of constitutive equations relating the three-dimensional electric field vector E , the three-dimensional electric displacement vector D , the six-dimensional stress vector σ , and the six-dimensional strain vector ϵ . [4]

$$\varepsilon_i = S_{i,j}\sigma_j + d_{m,i}E_m \quad (4)$$

$$D_m = d_{m,i}\sigma_i + \xi_{i,k}E_k \quad (5)$$

In matrix notation:

$$\varepsilon = S\sigma + dE \quad (6)$$

$$D = d^T\sigma + \xi E \quad (7)$$

S is the matrix of compliance coefficients, a 6x6 matrix whose members have units of square meters per Newton. These coefficients quantify how readily a material exhibits strain (a unitless value representing the change in length along one dimension over the original length) in response to stress. The permittivity matrix ξ can be expressed as square 3x3 square matrix for anisotropic materials. It quantifies the relationship between electric field and electric displacement; its elements have units of farad per meter. Note that these equations account for the well-understood relationship between stress and strain from solid mechanics, as well as the relationship between electric field and electrical displacement.

The unique property of piezoelectricity is encapsulated in the key parameter $d_{m,i}$, also known as the matrix of piezoelectric strain coefficients, or the matrix of piezoelectric charge constants. It has units of meters per volt (or equivalently, coulombs per newton) and quantifies the charge developed in response to applied stress, as well as the strain developed in response to applied electric field. Since this thesis seeks to develop an actuator—a device that converts an electrical signal into a mechanical response—this characteristic will be the focus when selecting

a suitable piezoelectric material. Viewing the relevant term of the equation in expanded matrix form helps to understand the nature of piezoelectric coupling.

$$\begin{bmatrix} \varepsilon_{1,1} \\ \varepsilon_{2,2} \\ \varepsilon_{3,3} \\ \varepsilon_{2,3} \\ \varepsilon_{3,1} \\ \varepsilon_{1,2} \end{bmatrix} = \begin{bmatrix} d_{1,1} & d_{1,2} & d_{1,3} & d_{1,4} & d_{1,5} & d_{1,6} \\ d_{2,1} & d_{2,2} & d_{2,3} & d_{2,4} & d_{2,5} & d_{2,6} \\ d_{3,1} & d_{3,2} & d_{3,3} & d_{3,4} & d_{3,5} & d_{3,6} \end{bmatrix}^T \begin{bmatrix} E_1 \\ E_2 \\ E_3 \end{bmatrix} \quad (8)$$

Within a range of linearity, the inverse piezoelectric effect produces strain in response to an applied electric field. Each three-dimensional component of the electric field contributes to one of the nine (six, in simplified form) components of strain. The sum of the contributions from each electric field component determines the total strain response.

Material Orientation

At this point it should be noted that the values of the elements of the piezoelectric strain matrix will depend on the choice of axes 1, 2, and 3; this means that the piezoelectric strain constants of a material vary based on the orientation of the material when these values are measured. Thus, it is necessary to have some common convention for orientation when specifying the piezoelectric properties of a material. The Institute of Radio Engineers (IRE), one of the predecessors to IEEE, published the first “Standards on Piezoelectric Crystals” in 1949. [8] Today, the more commonly used standard is that published by IEEE in 1978. [9] It defines the orientation of a piezoelectric material on the basis of its crystalline structure. Basis vectors 1, 2, and 3 are defined as equivalent to the positive x-axis, positive y-axis, and positive z-axis (respectively) in a right-handed Cartesian coordinate system. The positive z-axis generally corresponds with the direction of the positive dipole in a unit crystal cell. For a trigonal crystal such as lithium niobate, this corresponds with the axis of six-fold symmetry (the *c-axis* under the

Bravais-Miller system.) The x-axis is defined to correspond to one *a*-axes of symmetry, perpendicular to the c-axis. The y-axis is then defined to complete a right-handed, orthogonal coordinate system.

Device Fabrication

When incorporating piezoelectric materials into device fabrication, controlling the orientation of the material within the device is thus vital. There are several ways to incorporate piezoelectric materials into a wafer stack. They can be grown or deposited directly onto the substrate. For example, aluminum nitride (AlN) can be deposited on certain substrates using reactive sputtering. The resulting structure may be polycrystalline, creating isotropy within the plane of the device. However, most or all grains within the structure will grow in such a manner that they align their c-axis of symmetry with the z-axis, normal to the surface of the substrate. As a result, the piezoelectric coefficients of the resulting material layer will be isotropic within the plane of the device, but anisotropic in the direction normal to the device plane.

It is also possible to grow piezoelectric materials in a single-crystal bulk structure. This bulk structure can then be cut into thin layers that are then bonded to a substrate. Because the bulk crystal can be cut along an arbitrary plane, this allows substantial flexibility to select an appropriate orientation for the device. By convention, three basic orientations are defined with respect to the direction normal to the substrate (upwards and out-of-plane.) X-cut material will align the material so that the x-axis (as defined per the IEEE standards) is normal to the substrate, while the y-axis and z-axis are in the device plane. Y-cut and z-cut are defined similarly. Devices also use piezoelectric layers that are a set rotation from one of these standard

cuts; for example, surface acoustic wave (SAW) devices often incorporate lithium niobate (LiNbO_3) with a 128° off Y-cut.

(For simplicity, the vertical, out-of-plane axis with respect to the device substrate will hereafter be referred to simply as the z-axis; any reference to the crystallographic z- or 3- axis of the material will so specify explicitly. The two in-plane axes shall be referred to simply as the x-axis and y-axis, as indicated in the figure. Since this paper will primarily be discussing beam structures—and the most directly relevant parameter in understanding the operation of each beam is the crystallographic orientation of the piezoelectric material with respect to that beam, and the transformed piezoelectric coefficient matrix for that orientation—it also will be helpful to establish a convention with respect to the orientation of each beam unit. Thus, axis 1 will refer to the longitudinal axis, running along the longest in-plane dimension of the beam. Axis 3 will coincide with the z-axis of the substrate. Axis 2 will be orthogonal to both the longitudinal axis and the vertical axis; it will always lie in the plane of the substrate.)

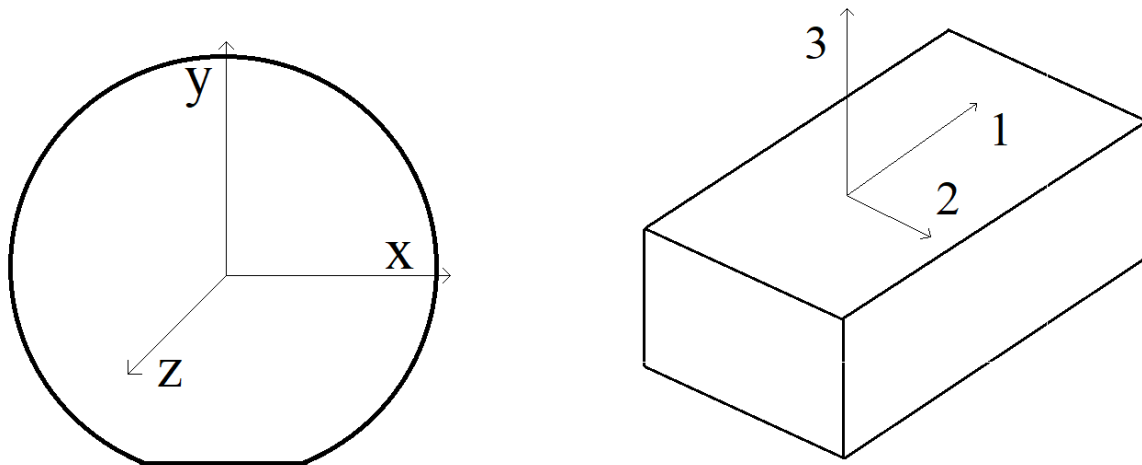


Figure 7. Axis orientation with respect to substrate wafer orientation (left) and with respect to MEMS beam orientation (right).

It is primarily the selection of a cut that determines how a layer of piezoelectric material can be utilized. This is because orientation piezoelectric crystal orientation with respect to the vertical z-axis is fixed. In contrast, it is generally trivial to rotate a piezoelectric structure within the plane of the device substrate (though other device components may introduce constraints.) Thus, it is possible to change the effective orientation piezoelectric material within each individual device. In a material such as sputtered aluminum nitride, which is isotropic with respect to the x-axis and y-axis of the device, the orientation of the piezoelectric components within the substrate does change their performance; this gives more freedom to reorient piezoelectric components to optimize other metrics without affecting their components. In a fully anisotropic material, such as single-crystalline lithium niobate, the orientation of each structure within the plane will change the piezoelectric coefficient matrix with respect to that structure, thus changing how the device will behave. While this introduces a constraint on the orientation of the piezoelectric structures, it also grants greater flexibility, permitting a variety of different behaviors within the same substrate layer. This project ultimately exploits this flexibility in order to develop improved actuators that take advantage of two distinct piezoelectric responses acting in concert.

CHAPTER THREE: BIMORPH BENDING BEAMS

Structure of Bimorph Beam

One of the simplest and most widely used solutions to the problem is to use a bimorph bending beam. This structure comprises two separate layers of piezoelectric material, or a single piezoelectric layer and a layer of linear elastic material with enough stiffness to resist the expansion or contraction of the piezoelectric material. The two layers are separated by thin-film layers of conducting material. These conducting thin-film layers act as electrodes, carrying an electrical signal to the bimorph structure. Because piezoelectric materials are generally dielectric, charge accumulates along the interface between the piezoelectric material and the conductor, applying a constant electric potential along each interface.

The major advantage of this design is simplicity. In the microfabrication process, building up a stack of different materials is straightforward, particularly when each vertical layer consists of only a single material. Moreover, because the conducting layers cover the entirety of the piezoelectric structures, after the stack has been built it is possible to pattern multiple layers in a single photolithography step, reducing the number of masks needed and the overall complexity of the process.

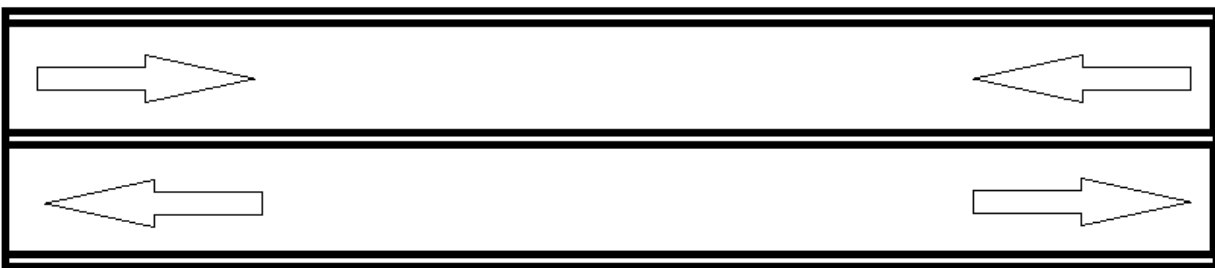


Figure 8. Diagram of simple bimorph beam.

The bimorph structure functions because each piezoelectric layer acts separately, with one layer expanding longitudinally while the other layer contracts along the same axis. Because the two layers are mechanically connected, this introduces stresses at their interface. As points on the surface of the expanding beam separate, they exert outward (positive stress) forces on the contracting beam, and the contracting beam exerts the opposite force on the expanding beam. These forces result in both normal stresses and shear stresses. The normal stress components primarily act to oppose the negative strain of the contracting beam, reducing the amount of contraction and oppose the positive strain of the expanding beam, limiting the amount of expansion. The shear stresses introduce a bending moment into the bimorph beam, causing the entire structure to curve towards the contracting layer. The precise relationship between the deflection and the strain of the two piezoelectric layers depends on the elastic stiffness of the material, the moment of area of the cross section of the structure, and other properties of the system; however, at MEMS scale, the bimorph configuration will often transform small, in-plane strain into comparatively large, out-of-plane deflections.

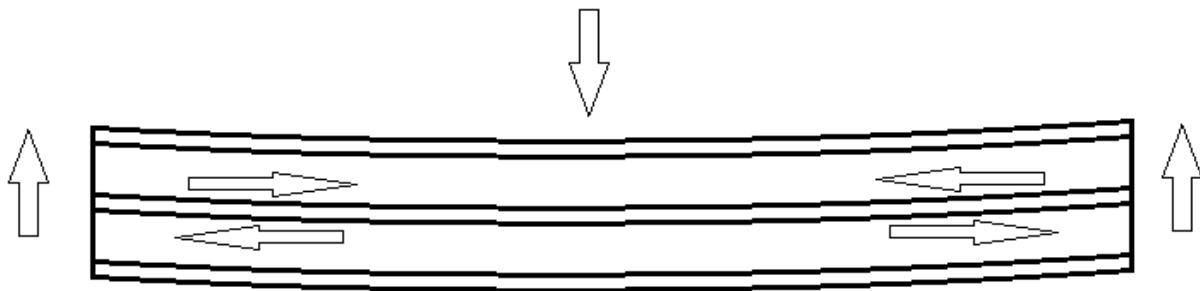


Figure 9. Unequal strain develops bending moment.

Electric Field Pattern

In order to achieve positive strain in one piezoelectric layer and negative strain in the other simultaneously, the two layers must have different crystal orientations, different applied electric fields, or both. Fortunately, a simple configuration can achieve the desired effect using two piezoelectric layers in the same orientation. Using the previously described electrode structure, a signal voltage can be applied to the middle conducting layer, while the remaining two electrodes are grounded. This results in a uniform electric field applied to the top piezoelectric layer. Simultaneously, a uniform electric field is applied to the bottom piezoelectric layer; this field will be equal in magnitude and opposite in direction. See Figure.

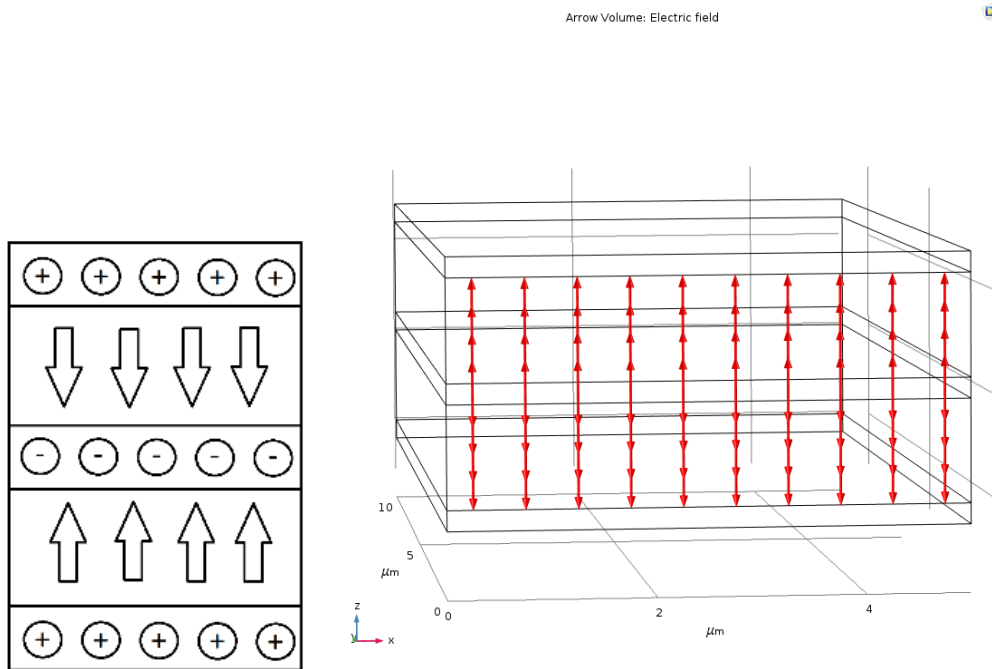


Figure 10. Cross sectional area of bimorph beam in larger structure.

These electric fields only have a z-component, or a component 3 with respect to the beam structure. Thus, this design works best with piezoelectric materials oriented to have strong $d_{3,1}$ coupling. Aluminum nitride possesses several favorable qualities for use in MEMS devices,

including process compatibility and the absence of rare or toxic components. It is particularly suitable for use in a bimorph beam because of its piezoelectric coefficients and orientation. As discussed in the previous chapter, sputtered aluminum nitride is isotropic in the plane orthogonal to its poling direction. This means that its piezoelectric charge matrix has several symmetrical values, and multiple zero values, taking the following general form. [5]

$$d = \begin{bmatrix} 0 & 0 & 0 & 0 & d_{1,5} & 0 \\ 0 & 0 & 0 & d_{1,5} & 0 & 0 \\ d_{3,1} & d_{3,1} & d_{3,3} & 0 & 0 & 0 \end{bmatrix} \quad (9)$$

While in-plane electric field components couple with shear strain, it is the electric field component normal to the substrate—the primary component generated by the bimorph design—that evolves normal strain. Moreover, because reactive sputtering deposits aluminum nitride with the poling direction normal to the substrate, it is simple to achieve the proper orientation within the device.

Surface: Total displacement (μm)

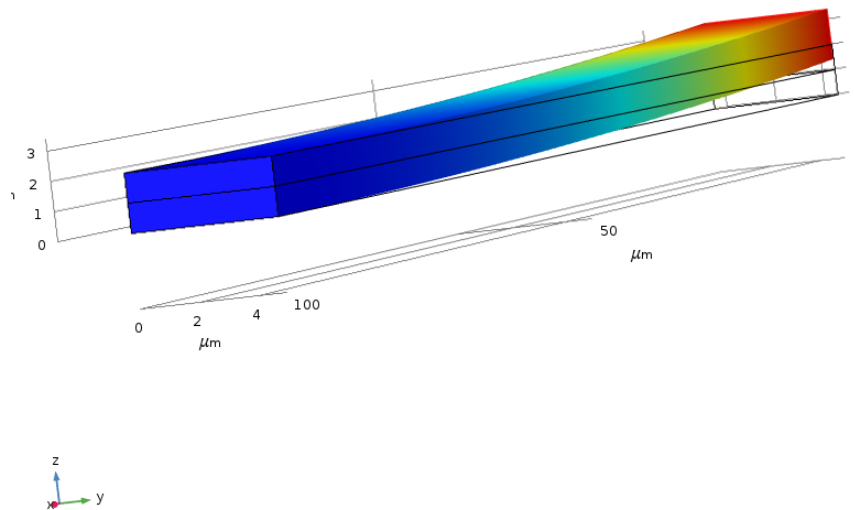


Figure 11. Displacement plot of bimorph aluminum nitride beam.

COMSOL software was used to simulate a bimorph aluminum nitride beam with dimensions 100 micrometers long by 5 micrometers wide by 2 micrometers high, a benchmark to measure against the performance of the unimorph design. With an applied electric potential of 10 V, this structure produced a 140 nanometer deflection over a 100 micrometer length. This deflection is typical for piezoelectric devices. While this may appear to be quite a small deflection relative to the dimensions of the device, modeling the behavior of each piezoelectric layer separately demonstrates how effectively the bimorph design amplifies much smaller displacements. As individual free beams, each piezoelectric layer develops just over 10^{-5} strain in the longitudinal direction, or roughly 2 nanometers of longitudinal movement.

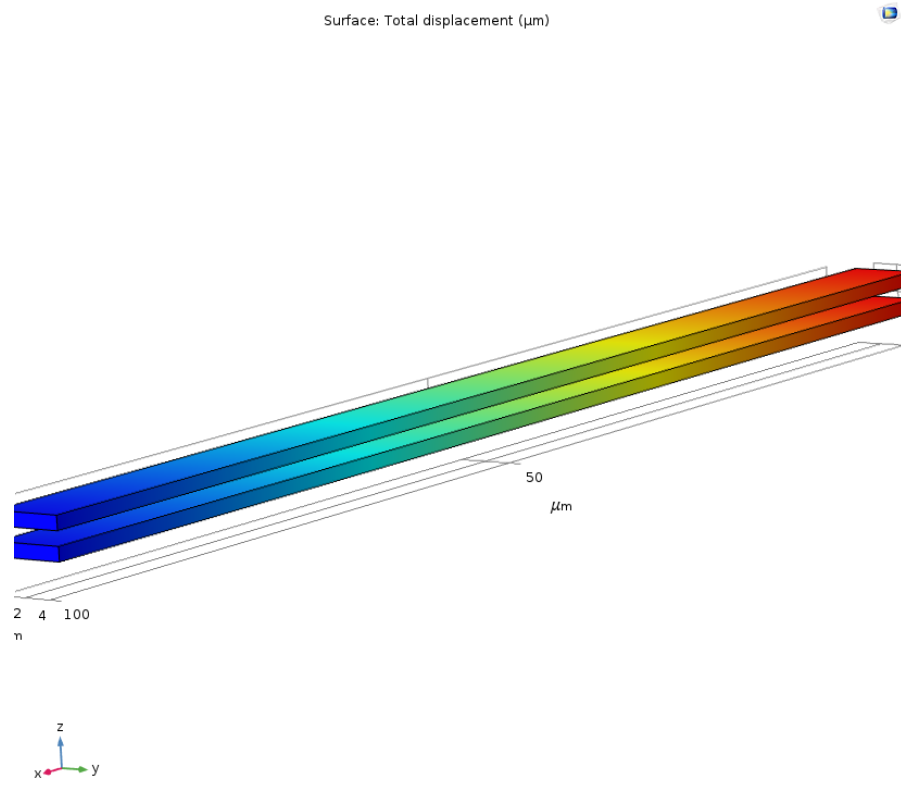


Figure 12. COMSOL model of individual aluminum nitride beams.

CHAPTER FOUR: NOVEL ELECTRODE PATTERN

Advantages of a Unimorph Design

The existing bimorph design presents several limitations. In order to create a bending moment, two portions of the beam must act in opposition—ideally, with one layer exhibiting positive strain (expanding), while the other exhibits negative strain (contracting) along the same axis. These components must be mechanically connected in order to move in tandem along their interface, but also electrically connected in such a way that a different electric field can be applied to each portion. The bimorph design applies an electric field to each layer that is uniform, but opposite in direction, causing the opposing strain. This simplifies both the fabrication process and the mathematical modeling. A uniform electric field can be applied with a simple structure: a uniform conducting thin film completely covering two opposing faces at different potentials.

Causing a bending moment with a single piezoelectric layer would present significant advantages. When incorporating a piezoelectric layer into a stack—and in microfabrication in general—a substantial portion of the costs come not from the acquisition or manufacturing of the material, but from the processing of each layer. Even using a comparatively expensive piezoelectric material such as lithium niobate, most of the cost of fabrication comes processing, and not material. Each layer added to the wafer stack may involve cleaning or otherwise preparing the substrate, material deposition or growth on that substrate to a precise thickness, or bonding material to the substrate and etching or polishing down to the desired thickness and finish. Furthermore, patterning each layer as a distinct structure adds additional photolithography steps. For each of these processes, labor, reagents, and equipment time adds to the direct costs of

fabrication. Moreover, every step of processing introduces another chance of breakage, misalignment, or contamination; this in turn reduces yield, increasing the cost per unit in industrial processes, and introducing delays and confounding variables in research. In short, working with one layer of piezoelectric material—even if that layer is several times thicker, or comprised of a different, more expensive material—would likely result in lower costs than a similar design calling for two thinner but distinct layers of a less expensive material.

Even if cost, manufacturing time, and yield were not considerations, reducing the number of layers presents other significant advantages. In microfabrication, there is always the potential for stress at the interface between two different materials, particularly when there is a substantial difference between the average operating temperature and the temperature during the bonding or deposition process. At macro-scale, the magnitude of these stresses tends to be small compared to the stiffness of the structures involved, and they tend to affect primarily the material near the surface, having minimal effect on the bulk material. At micro-scale, however, the surface to volume ratio increases drastically, and the magnitude of these stresses can be large enough to damage the device, or at least substantially influence their operation. Reducing the number of these interfaces reduces the potential for stress.

Operation of Novel Electrode Pattern

The advantages of unimorph design are thus clear, but the question is how it would be possible to create a bending moment in a single contiguous piece of material? The simplest solution is to apply a non-uniform electric field, causing different portions of the piezoelectric material to experience a different local electric field, and thus exhibit different local strain.

Surface acoustic wave (SAW) devices, for example, have achieved non-uniform electric fields using a comb pattern to excite resonant modes in a piezoelectric structure.

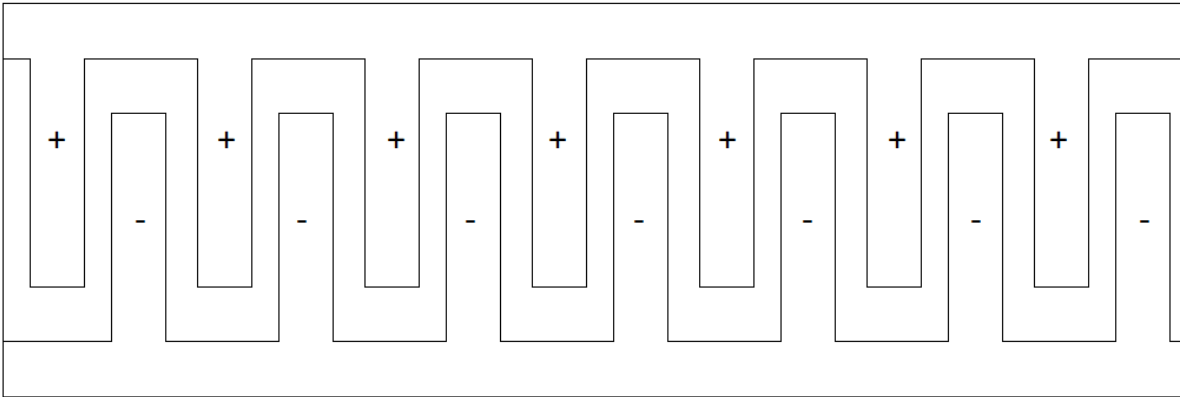


Figure 13. Top view of signal electrodes for SAW device.

However, this configuration does not produce the desired non-uniform electric field pattern to mimic the behavior of a bimorph beam. In order to achieve an out-of-plane bending moment, the electric field must change substantially along the z-axis—this is how the top piezoelectric material will exhibit different behavior from the bottom material. Moreover, this thesis seeks to achieve an actuator design. Though it may be possible to adapt these designs for use as a resonator, actuators have one key distinction: They must respond to signals with substantial DC components. Primarily, this requirement prevents the direct adaptation of the SAW design: The repeating pattern of the combs generates a similarly periodic electric field that repeatedly inverts.

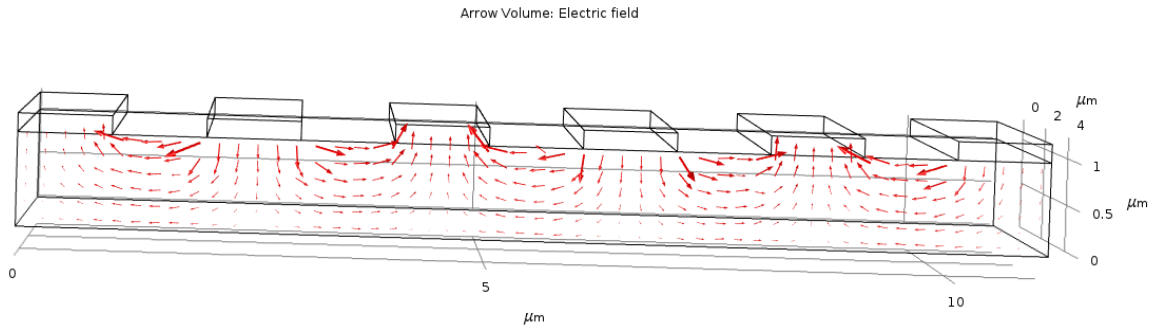


Figure 14. Electric field pattern along longitudinal cross-section of surface acoustic wave (SAW) pattern beam.

Taking a contour integral of the electric field along any line parallel to the longitudinal axis will yield a value that is zero or close to zero. Because the strain of the piezoelectric material is a linear function of the electric field, this means that the regions of positive strain largely balance out the regions of negative strain. This means that the comb pattern cannot produce the most important component of bimorph bending: substantial longitudinal strain.

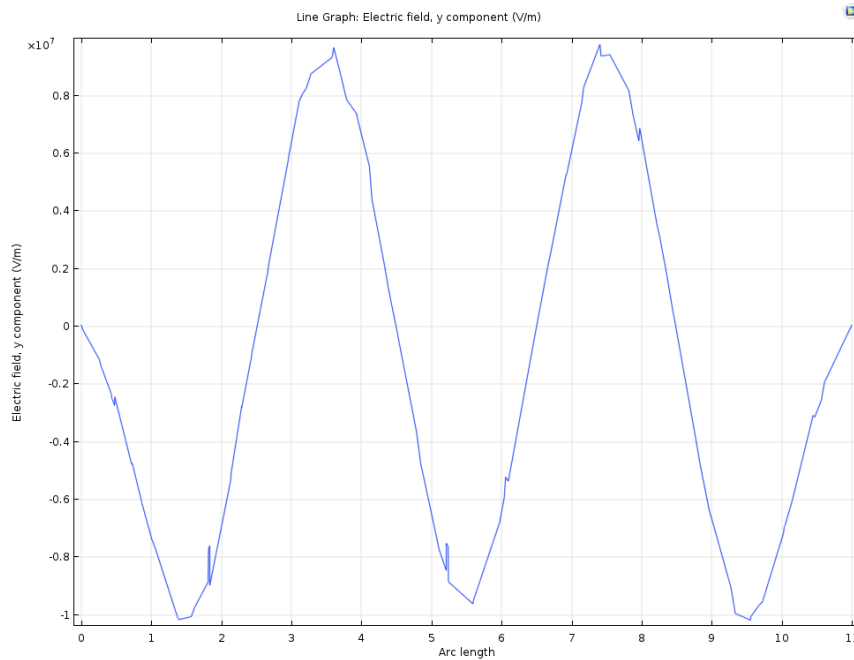


Figure 15. Plot of longitudinal (axis 1) component of electric field along length of SAW beam.

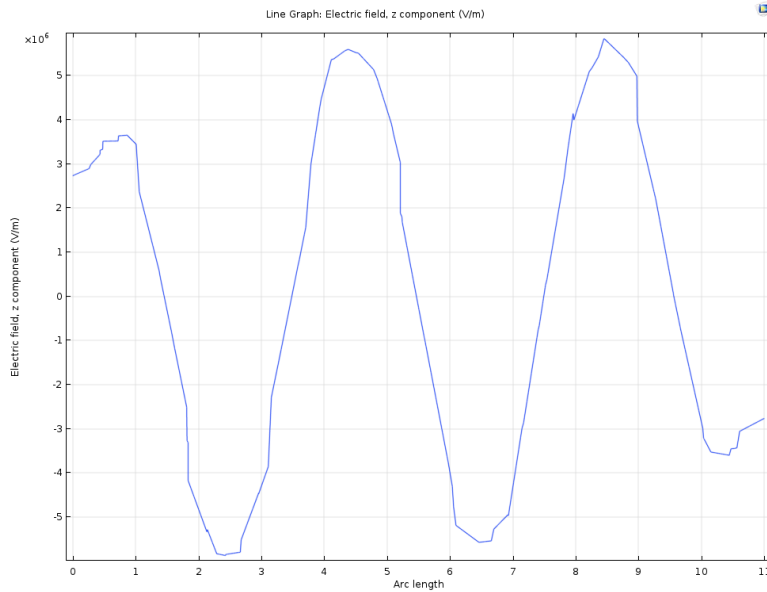


Figure 16. Plot of z-axis (axis 3) component of electric field along length of SAW beam.

A properly designed electric field pattern could cause the unimorph piezoelectric beam to act as a quasi-bimorph beam, with material closer to the bottom of the beam exhibiting positive strain, while material near the top of the beam exhibits negative strain. This means that there must be a substantial difference between the electric field near the upper face of the structure and the electric field near the bottom face. Moreover, the electric field must exhibit a consistent bias towards a particular polarity when moving longitudinally along the beam. Ideally, the bias along a line draw close to the top surface should be different from the bias along lines near the bottom.

One way to apply such a non-uniform field would be to place electrodes on the lateral faces of the beam. These electrodes would run along the entirety of the length of the beam structure, avoiding the problem of net-zero bias presented by a periodic pattern such as the SAW beam. Moreover, by controlling the location of the electrodes on the side way, a different bias can be focused on the top and the bottom portions of the piezoelectric layer. In the following

Figure, a positive bias signal is applied to an electrode on the upper left sidewall of the beam, while a ground electrode is placed opposite, on the upper right sidewall. Closer to the bottom of the beam, this configuration is reversed, with the lower left electrode acting as ground and the lower right electrode acting as positive bias. This creates a non-uniform field, with a negative bias along axis 2 (lateral, towards the left in the below Figure) near the top, and a positive bias along that same axis near the bottom. This is not an ideal configuration: Not only is the axis 2 electric field component weaker near the middle of the beam, there are substantial electric field components along axis 3 (the z-axis) near the sidewalls of the beam. This could introduce unwanted stresses into the device—while the ideal bimorph exhibits constant longitudinal strain within each piezoelectric layer, these unwanted electric field components may trigger unwanted normal strain or even shearing.

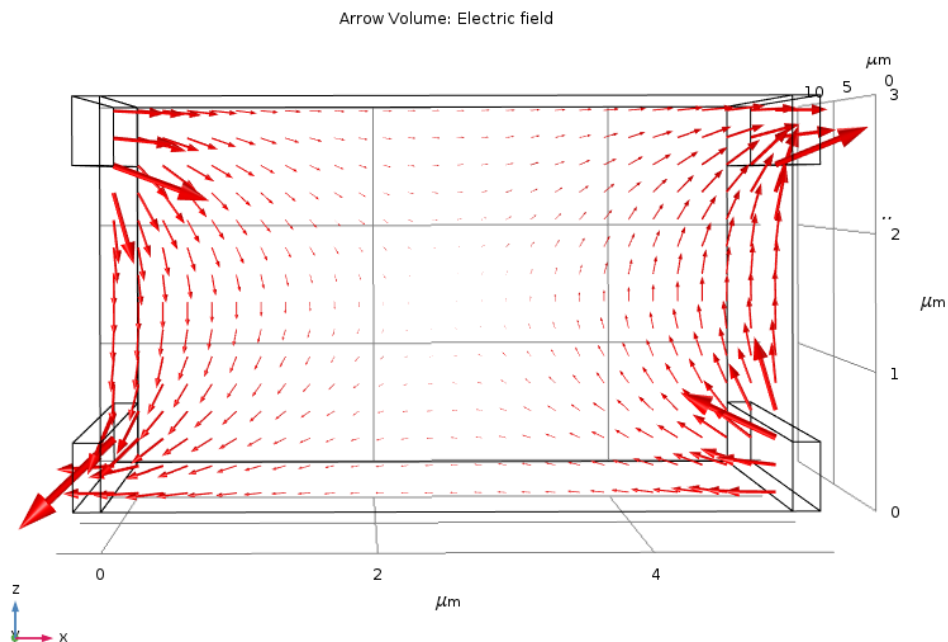


Figure 17. Electric field arrow plot along lateral cross-section of beam with laterally placed electrodes.

Furthermore, sidewall deposition in microfabrication, while possible, presents substantial complexity. The great strength of modern microfabrication techniques is the ability to process numerous device components in parallel using photolithography—however, most patterning and deposition processes work best in a top-down manner. While it is possible to achieve sidewall coverage using metal deposition techniques, maintaining uniformity among thousands of devices arrayed atop an angled wafer is a challenge. Moreover, photolithography generally patterns devices through use of a patterned mask on top of the substrate. This mask directs the processing of the underlying wafer stack by controlling the points where various batch processes can reach the substrate. This technique can achieve micrometer resolution when applying a pattern to the top of a wafer stack—however, it cannot achieve similar precision patterning lateral surfaces.

Instead, a non-uniform electric field was achieved modification of the top and bottom conducting layers. Because the existing processes already include the deposition of these layers, the only added complexity are steps to pattern these layers, using well-established photolithography techniques. Rather than covering the entirety of the beam with a uniform thin film at a single potential, two separate electrodes run longitudinally along the top surface of the piezoelectric beam. Held at different potentials, this forms a non-uniform electric field in the piezoelectric material. Closer to the surface, the electric field is dominated the component running tangential to the surface and normal to the direction of the beam. Two identical electrodes running on the lower surface of the beam, with reverse polarity, can create a similar effect, with a tangential field component that is opposite in polarity. (See next Figure.)

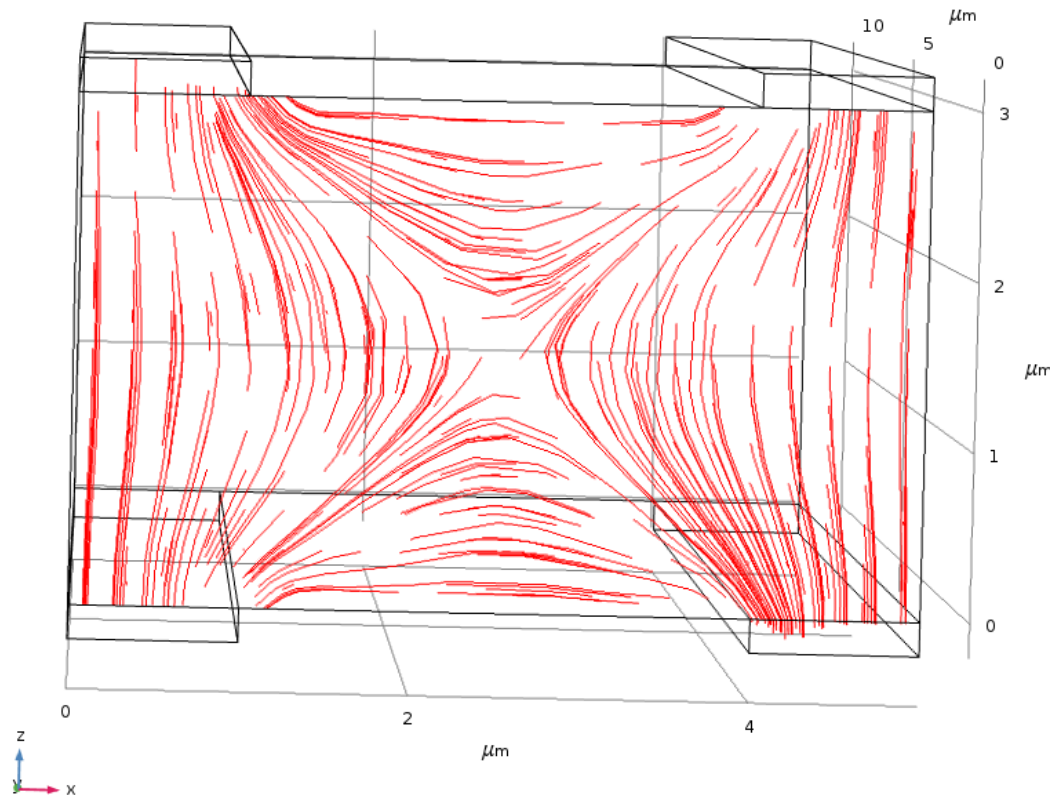


Figure 18. Plot of electric field lines on lateral cross-section of beam with top and bottom twin electrodes.

An arrow plot of this same cross-section better shows the reversal in direction of the lateral electric field components between the top and bottom surfaces of the piezoelectric

material.

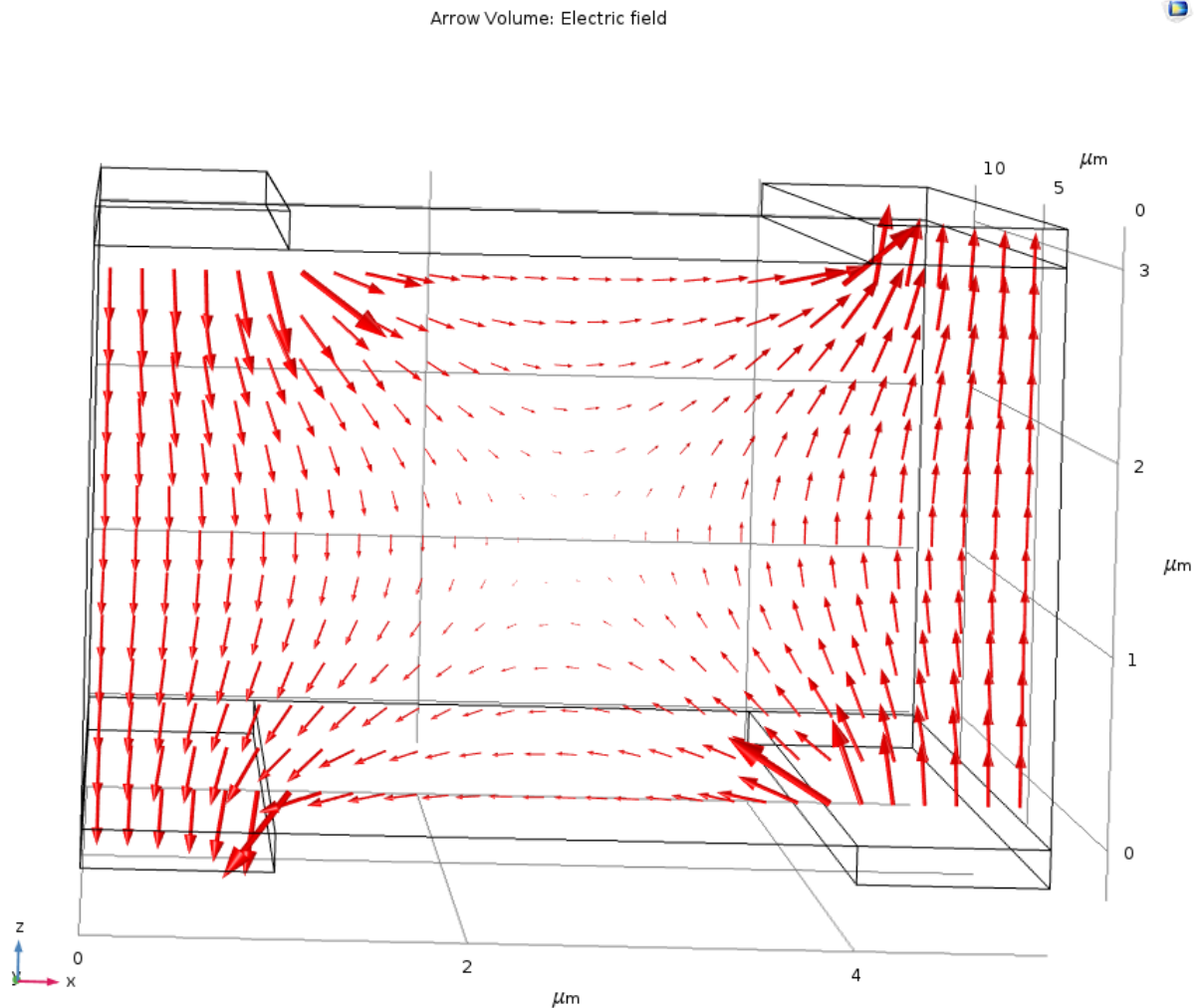


Figure 19. Arrow plot of electric field on lateral cross-section of beam with top and bottom twin electrodes.

Viewing the electric field in this manner reveals another complication: There is a strong positive electric field component in the z-direction on one side of the beam, and an equally strong negative electric field component on the other side. Recall from the discussion of the bimorph beam that this electric field component was the primary driver of the bending moment in aluminum nitride, which had strong $d_{3,1}$ and $d_{3,2}$ coupling. If this beam were fabricated using sputtered aluminum nitride, the substantial strain differential would create an in-plane bending

moment. While such a response has potential uses, for the purposes of this project it is unwanted behavior. Moreover, this problem cannot be solved simply by changing the orientation of the aluminum nitride. As previously discussed, sputtered aluminum nitride grows with the poling axis lateral to the surface—the equivalent of z-cut. Selecting another orientation would require finding a source that grows single-crystal aluminum nitride and bonds it to substrates. Such sources may be difficult to find due to the relative ease and widespread use of aluminum nitride sputtering. Moreover, recall that sputtered aluminum nitride has a small, but non-zero value for $d_{1,5}$ and $d_{2,4}$. This indicates that—even if the aluminum nitride were reoriented to align with the lateral (axis 2) electric field component, the unwanted vertical (axis 3) component would still cause shearing stress components. This is particularly problematic because the axis 3 component of the electric field is somewhat higher than the magnitude of the axis 2 component. Thus, in order to continue with this design, it is necessary to identify piezoelectric materials with more favorable properties.

CHAPTER FIVE: LITHIUM NIOBATE

Selection of Lithium Niobate

Again drawing inspiration from SAW devices, this project explored the suitability of lithium niobate as an alternative piezoelectric material. Grown in single-crystal structures, lithium niobate is readily available in various cuts for use in microfabrication, allowing more flexibility to find an orientation that suits the needs of this design. Moreover, SAW devices using a configuration similar to the one discussed in the previous chapter rely on the coupling of an in-plane electric field to excite ultrasonic waves along the same axis (the equivalent to $d_{1,1}$ with respect to the beam.) Thus, it is already established that there exist cuts of lithium niobate that can couple in-plane electric fields to in-plane strain components.

The piezoelectric properties of lithium niobate are well-studied, and various groups have measured and published the piezoelectric strain coefficients. These figures follow the IEEE standards, with axis 3 aligning with the positive dipole direction, and axis 1 determined by a plane of mirror symmetry. Though these characteristics do show some dependence on temperature and other factors, the published figures are considered accurate enough to use for mathematical modeling. [10]

$$d = \begin{bmatrix} 0 & 0 & 0 & 0 & 6.92 & -2.08 \\ -2.08 & 2.08 & 0 & 6.92 & 0 & 0 \\ -0.085 & -0.085 & 0.6 & 0 & 0 & 0 \end{bmatrix} \times 10^{-11} \frac{C}{N} \quad (10)$$

From these figures, it is clear that standard z-cut lithium niobate has strong shear coupling coefficients. This could potentially complicate the design, as the proposed electrode

pattern relies on the differential in the tangential electric field components to drive normal strain in order to produce a bending moment. Both in-plane field components couple strongly to shear strain, but not to normal strain. However, this orientation also demonstrates substantially weaker coupling with the axis 3 component of electric field—this behavior would help to mitigate the impact of the strong vertical electric field components near the sidewalls of the beam. Thus, there potentially exists an orientation where the piezoelectric coupling can work in concert with the electric field pattern produced by this unimorph configuration. Furthermore, lithium niobate offers additional advantages. As a single-domain crystal, lithium niobate should be free of hysteresis, the internal stress that can develop in a multigrain material such as aluminum nitride. Moreover, there is some existing literature on characterizing and processing lithium niobate, as other MEMS devices have incorporated lithium niobate, which additionally has interesting pyroelectric properties. This means that designing a fabrication process for a lithium niobate device does not have to be done entirely without guidance.

With these advantages and the potential for interesting behavior at varying orientations, lithium niobate seems to be a good choice for the unimorph device. Even more encouragingly, a recently published paper demonstrated the feasibility using lithium niobate in a traditional bimorph actuator, using a rotated cut to maximize the desired coupling. [11]

Rotated Piezoelectric Strain Coefficients

The group designing the lithium niobate bimorph beam derived expressions for the rotated piezoelectric strain coefficients in terms of angle of rotation from standard Y-cut, in order to maximize the desired normal strain coupling to their applied electric field, while minimizing the shear strain components generated by that same electric field. Though their design requires

were different than those of the present project, their work demonstrated that by selecting the proper crystallographic orientation, it is possible for a strong shear strain coupling coefficient to present as a strong normal strain coupling coefficient with respect to that orientation. [11]

More generally, it is possible to analyze the behavior of piezoelectric materials at various device orientations by examining their transformed electromechanical properties: compliance matrix s , permittivity matrix ϵ , and piezoelectric strain matrix d . Of these properties, the anisotropy of the piezoelectric strain coefficients most significantly drives the orientation dependence of lithium niobate. The piezoelectric strain matrix follows the transformation rules for third-order tensors and can be transformed to an arbitrary orientation using the rotational transformation matrixes for three Euler rotations about the original axes and the bond strain transformation matrix. [12]

However, this presents an impracticably large search space for an optimization problem as the orientation of the material has three degrees of freedom. Moreover, at this point in the design process, there is no precise statement regarding how to optimize the six elements of d . Because the cited lithium niobate bimorph design utilized uniform electric fields with only axis 3 components, it was able to focus on maximizing the $d_{3,2}$ component and minimizing the $d_{3,4}$ component. Because there the electric fields had no tangential components, there was no need to optimize the piezoelectric strain coefficients coupling with those components. The present design generally requires that the impact of the vertical (axis 3) electric field component should be minimized. Moreover, an in-plane electric field component should couple strongly to an in-plane strain component, preferably an orthogonal component. Unwanted strain components resulting

from that same in-plane electric field component should be minimized. Unfortunately, this is not precise enough to design an algorithmic search of the entire search space.

Instead, it is helpful to introduce practical constraints to simplify the problem. Looking ahead to prototyping this design, it is important to consider the availability of piezoelectric materials for fabrication. The lithium niobate used in microfabrication must be cut into thin slices from bulk material, so there is less wastage when producing many flats in the same orientation than there is when producing a few wafers in uncommon cuts. Thus, the material may be less expensive and more readily available when using more commonly used orientations. These orientations include the standard x-cut, y-cut, and z-cut, as well as a few commonly used angled cuts. However, from a starting cut, it is simple to explore different rotations about the z-axis (with respect to the wafer.)

COMSOL software was used to model the behavior of the unimorph beam at various in-plane orientations within several commercially available orientations of lithium niobate: x-cut, y-cut, z-cut, 38° off y-cut, and 128° off y-cut. The initial height of the model beam was 2 μm , based on a survey of the thinnest on-wafer layer commercially available. A proposed application for this design dictated rough constraints for the other dimensions: The initial model would be 5 μm wide and 100 μm long.

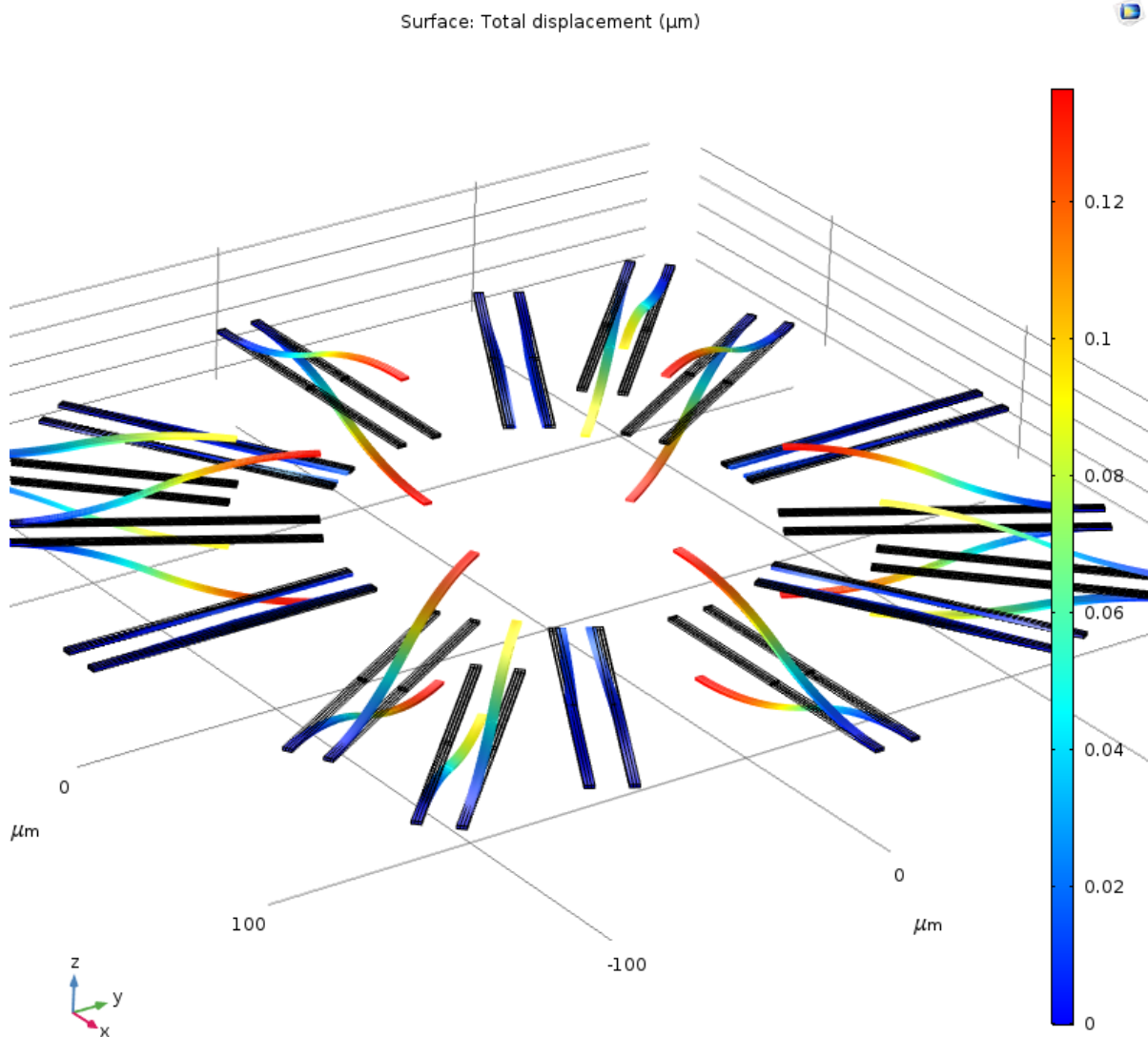


Figure 20. COMSOL model of unimorph beams at varying orientations within the x -cut plane. (Rotated coordinate system used for piezoelectric model.)

COMSOL modeling helped to visualize the total effect of the piezoelectric coupling, rather than just considering individual strain components in the abstract. Additionally, parametric sweeps of test structures throughout rotated orientations helped to reveal the effect of the interaction of desired strain components with unwanted strain components across different orientations. In some cases, total upward deflection was maximized at an orientation where the

desired piezoelectric strain constant was not maximized; the interaction with undesired coupling components unexpected improved performance.

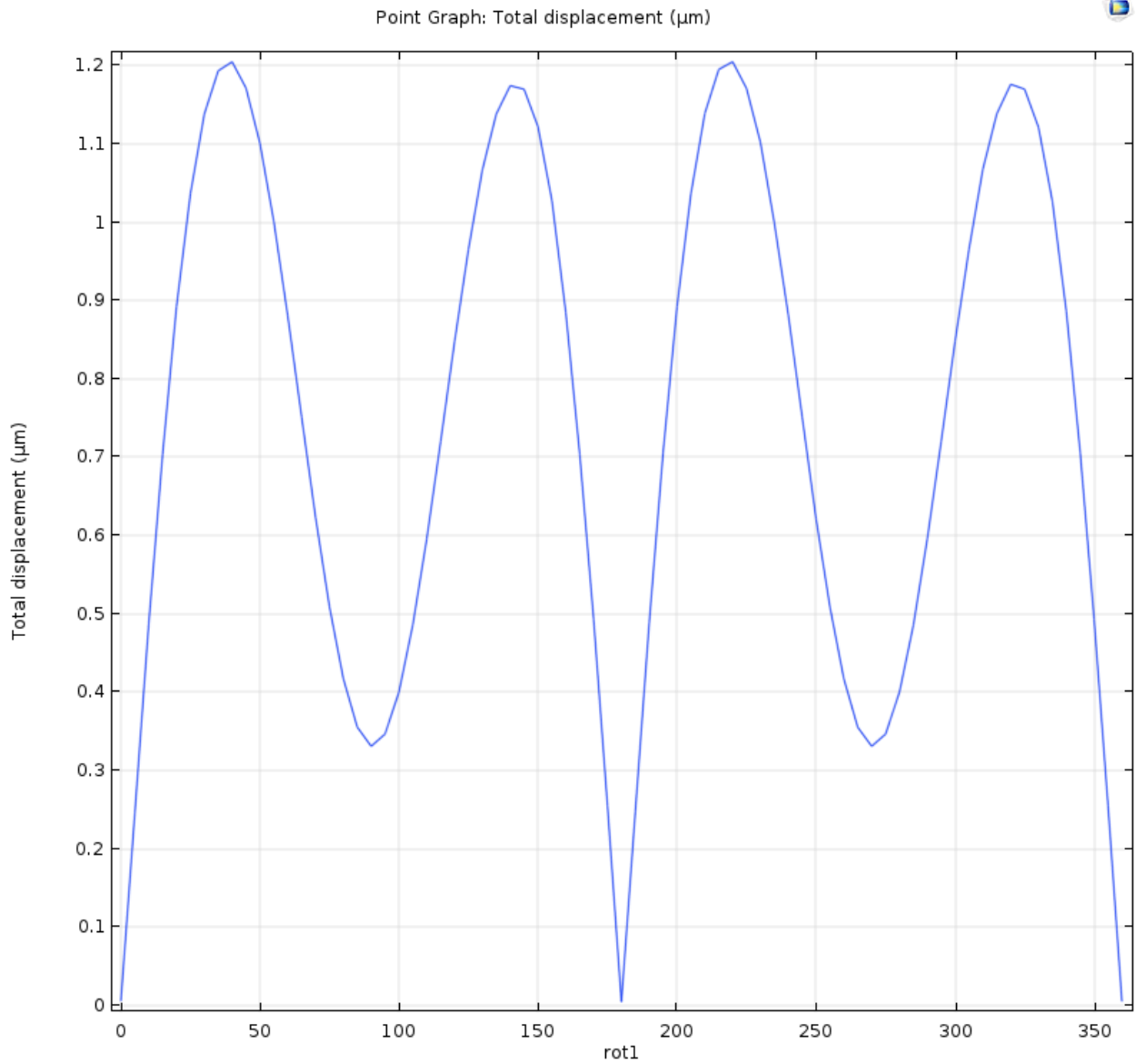


Figure 21. Parametric sweep of the total deflection of a test structure rotated about the x-axis.

Neither symbolic analysis nor COMSOL modeling yielded an ideal orientation with strong $d_{1,2}$ or $d_{2,1}$ coupling and no unwanted strain components among the simple transformations (in-plane rotation about the normal axis) from the common cuts. However, in some orientations,

the desired strain coefficients were significantly larger than the unwanted components; it was decided to explore whether the device design could compensate for those unwanted components. The most promising orientations were rotations of the x-cut. The tangential electric field (axis 2) component generated by the dual electrode patterns was able to produce sufficient longitudinal strain to form a bending moment. The magnitude of the bending far exceeded the performance of the aluminum nitride bimorph simulation—which had similar dimensions—from the previous chapter. Moreover, the magnitude of the bending deflection far exceeded the unwanted strain components, particularly at 40° and 220° rotations in-plane. However, it was this unwanted strain that proved to be more interesting.

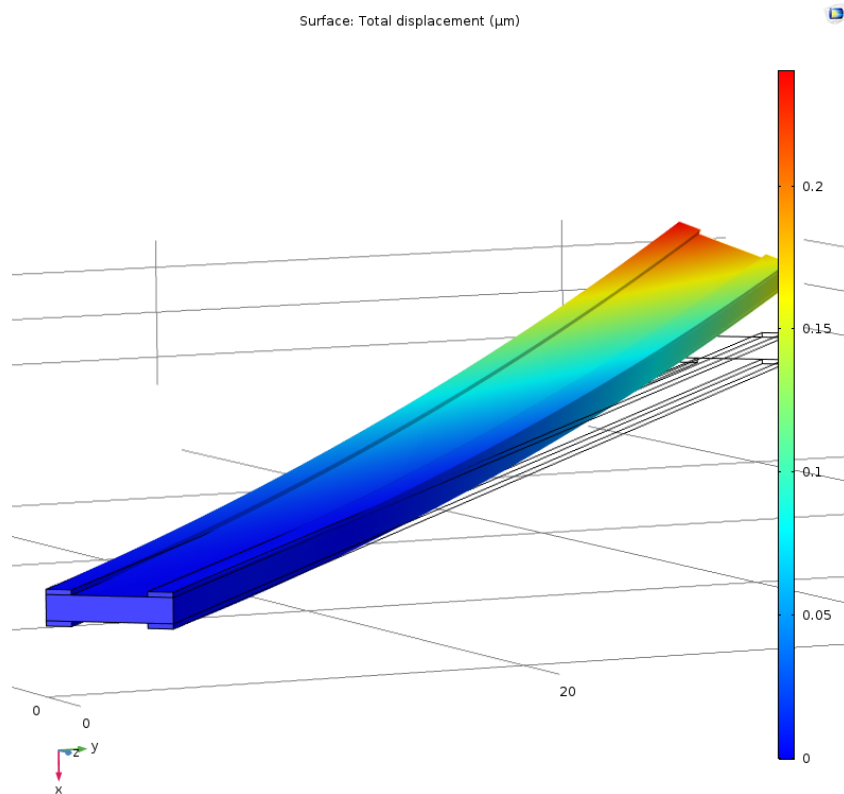


Figure 22. Model of test structure in x-cut lithium niobate, displaying bending and twisting components.

CHAPTER SIX: UNIMORPH BEAM DESIGN

Torsion Actuation

A significant $d_{3,6}$ and a strong vertical (axis 3) electric field component near the sidewalls coupled resulted in substantial shearing (strain component $\epsilon_{3,1}$) near the sidewalls. At the opposite lateral face, the axis 3 electric field component has the opposite polarity, causing the opposite shearing strain. Much like how the unequal normal strains evolve a bending moment, these unequal shearing strains evolve a torsional response about the longitudinal axis. This response exists to some degree in all x-cut orientations. Perhaps most noteworthy, at 130° rotation in-plane and periodically, the torsional behavior becomes the dominant response as the bending moment is significantly diminished. Coincidentally, this orientation is close to perpendicular to the bending orientation, within the plane of the device.

This operating mode has the potential for interesting applications—notably, controlling the angle of a reflector might have utility in displays or LIDAR. For the present design goal—achieving substantial out of plane actuation—this behavior may still be useful. By connecting the torsion actuator perpendicularly to a cantilever beam, this structure can produce an out-of-plane deflection.

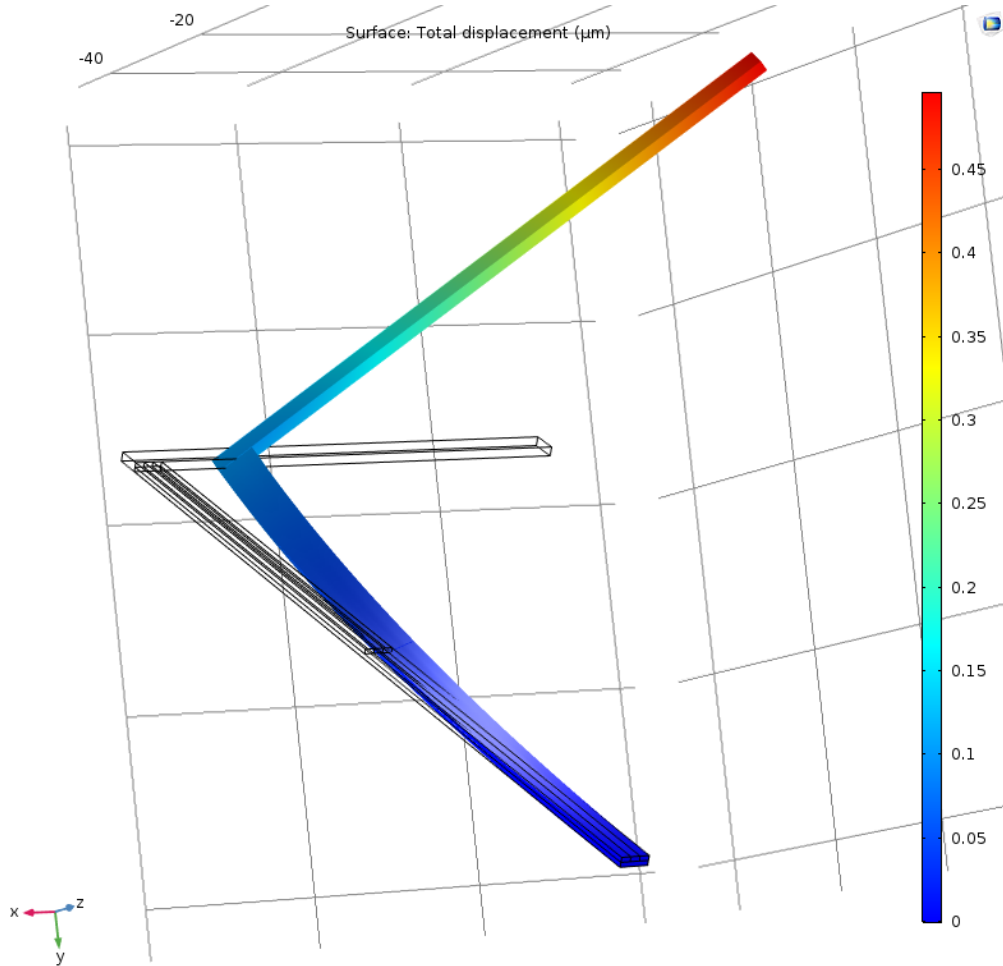


Figure 23. Model of torsion beam actuator with perpendicular cantilever beam.

This structure can achieve substantial deflections. The prior Figure demonstrates one of the torsional configurations discovered earlier in this project. Even though the dimensions of this model are not optimized, it produces an upward deflection of 450 nanometers, well above the performance of the aluminum nitride bimorph beam. The primary limitation of this design is device footprint. The angle of the cantilever beam is roughly proportional to the length of the torsion beam; the linear deflection is proportional to the length of the cantilever beam.

Bending Actuation

Taking advantage of the three-axis anisotropy of lithium niobate, it is possible to select an orientation where the transformed d_{31} is the dominant piezoelectric coefficient. This means that the opposing tangential electric fields cause strain along the longitudinal axis of the beam. By properly setting the polarity of the electrodes, the device can cause negative strain near the top of the material, and positive strain near the bottom, causing an upward bending moment. Around 40° rotation in-plane, and periodically, the bending moment dominates the response of the beam, though some torsional response remains.

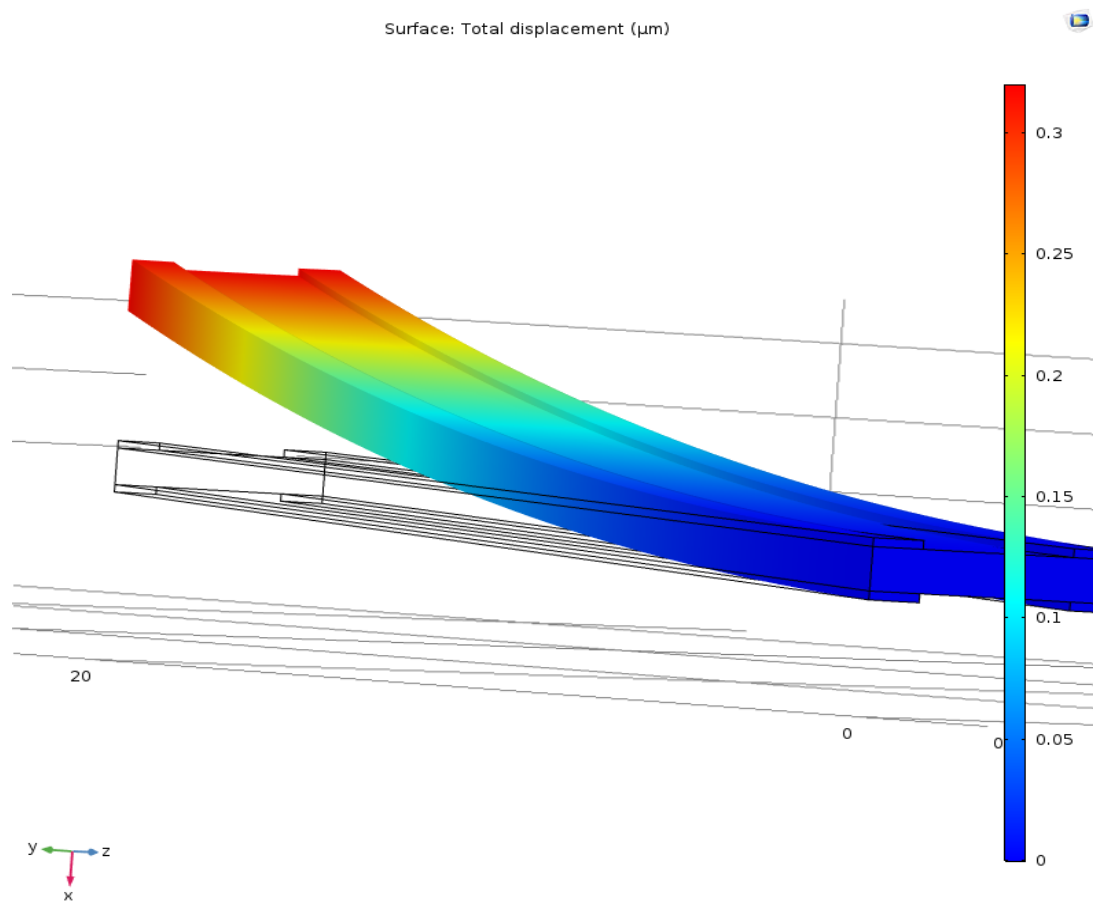


Figure 24. Unimorph bending actuator.

In the previous Figure, the unimorph beam achieves twice the deflection of a comparable bimorph design. Moreover, much like a bimorph design, this unimorph bending beam can be incorporated into a multistage structure to achieve larger total out-of-plane displacements. This meandering configuration effectively fits a longer beam into a smaller device footprint.

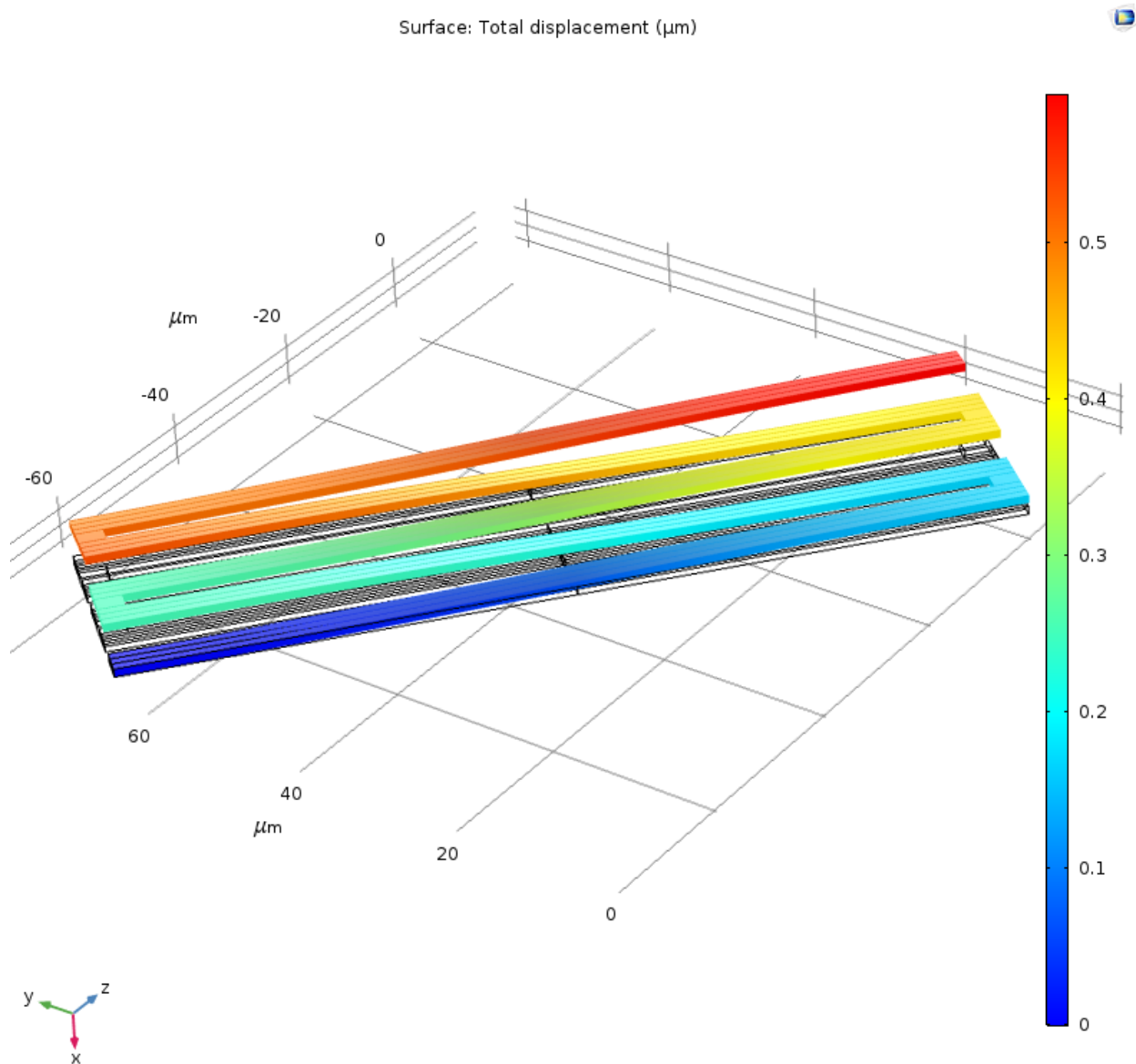


Figure 25. Initial bending multistage actuator design.

However, implementing this multistage design revealed two flaws in the current bending beam design. First, the small torsional response that remained even at the optimal x-cut orientation would be amplified over multiple stages, potentially presenting problems with device operation. Second, for each individual beam, the upward curvature throughout the beam creates not only upward deflection, but also an upward angle. In this multistage configuration, this angle actually tilts the subsequent stage downward, reducing the potential vertical displacement gained by that subsequent stage. Both issues are resolved by reversing the polarity of the electric field halfway along the beam.

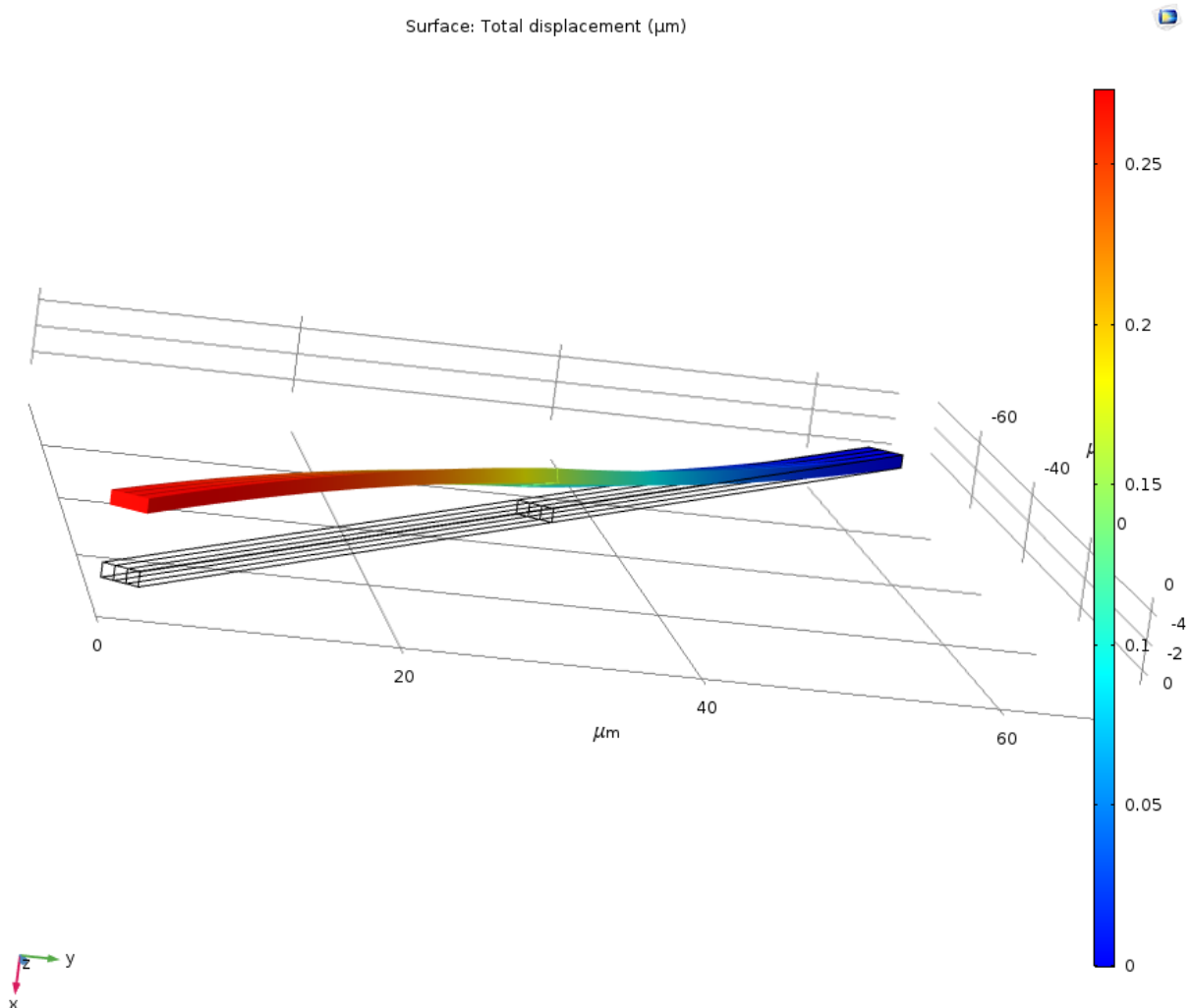


Figure 26. Model of bending beam with reversal of polarity.

Reversing the bending moment slightly reduces the total gain in vertical displacement, but also reverses the curvature and prevents the detrimental angle in the previous design. Moreover, the longitudinal torsion is also reversed, meaning that the moving tip of the actuating beam remains largely level.

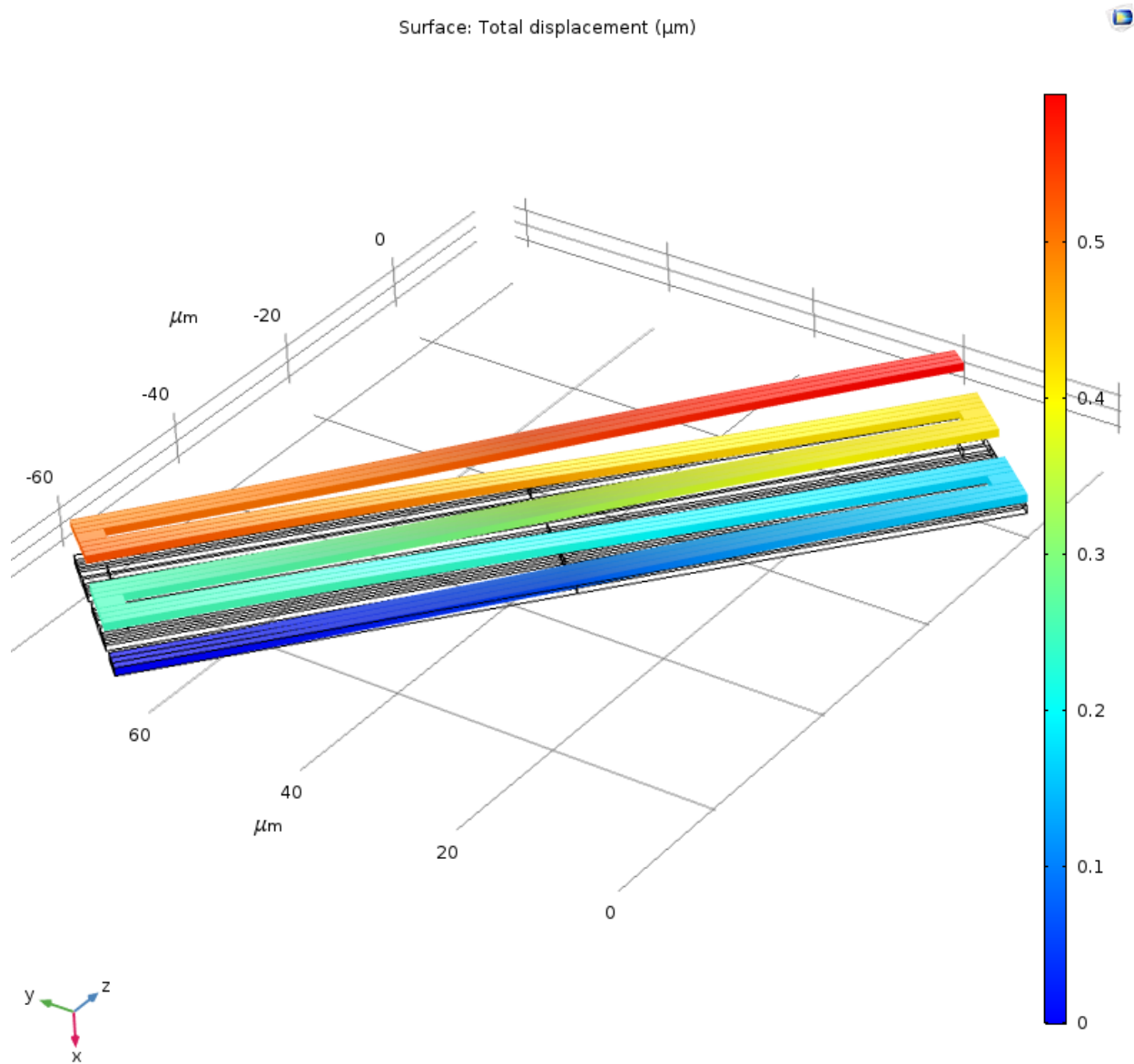


Figure 27. Multistage bending beam actuator with reversals.

However, there is one serious problem with this solution: It would require that the ground electrodes and the signal electrodes cross over one another on the same surface. Piezoelectric actuators such as this are free-floating. Thus, any electrical signal sent further along the device must be sent along the length of that device. The difficulties of sidewall metallization have already been discussed; any other solutions would likewise be complicated from a fabrication standpoint. Instead, it may be time to revisit the electrode pattern design.

Electrode Pattern Revision

The dual electrode pattern provided strong performance in a single beam but now limits flexibility in designing complex structures. If a simpler electrode pattern could generate a similar non-uniform electric field with the changing E_2 component, then the same orientation could be used to produce a similar response. Additionally, this presents an opportunity to address an unexpected complication: Bonding lithium niobate to a substrate with a patterned metal thin-film may introduce complications into the process, as does attempting mask alignment through a continuous lithium niobate layer after it is bonded. Using a single bottom electrode would also simplify the fabrication process.

The electrode pattern was first modified by creating a continuous ground electrode on the lower surface of the beam, replacing the dual ground electrode and signal electrode. Plotting the electric field pattern for the lateral cross-section showed a very different pattern. However, the most important features remained. The quasi-bimorph behavior is driven by the differential in the lateral axis 2 electric field. In the original design, that component is roughly equal in magnitude and opposite in polarity in comparison to a point on the opposite surface of the beam. Thus, where a point near the top of the material experiences negative strain, the corresponding point

near the bottom of the beam experiences positive strain, creating the bending moment. A similar differential exists in the revised design. While the dual electrodes on the top surface cause a substantial lateral electric field, that electric field component approaches zero near the lower surface. This is unsurprising, as metal (platinum, in the case of this simulation) is as close to a perfect conductor as exists in nature, and it is well-known that tangential electric field components vanish along the interface with a perfect conductor.

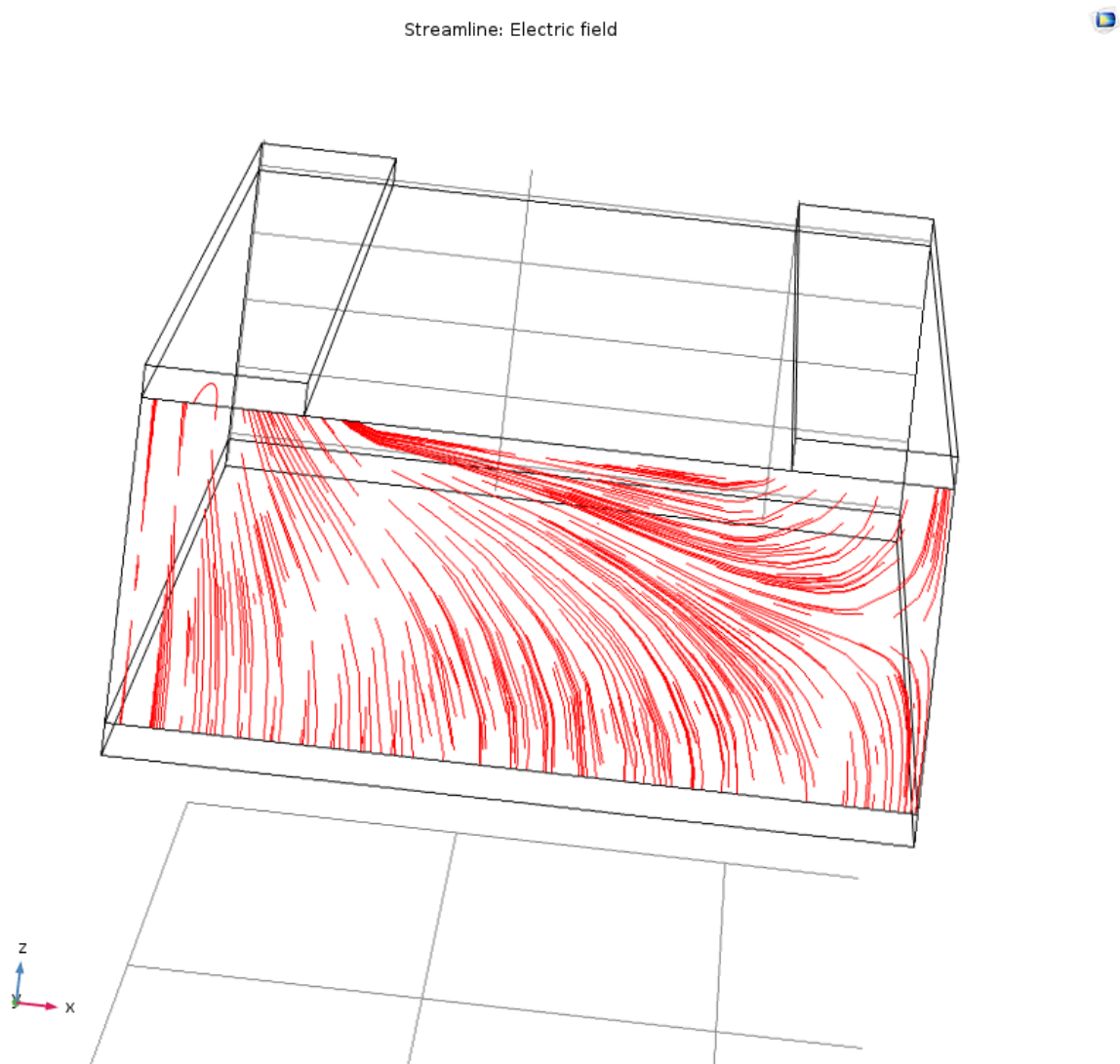


Figure 28. Streamline plot of electric field along lateral cross-section of unimorph beam. (Dual top electrodes: signal and ground. Single bottom electrode: ground.)

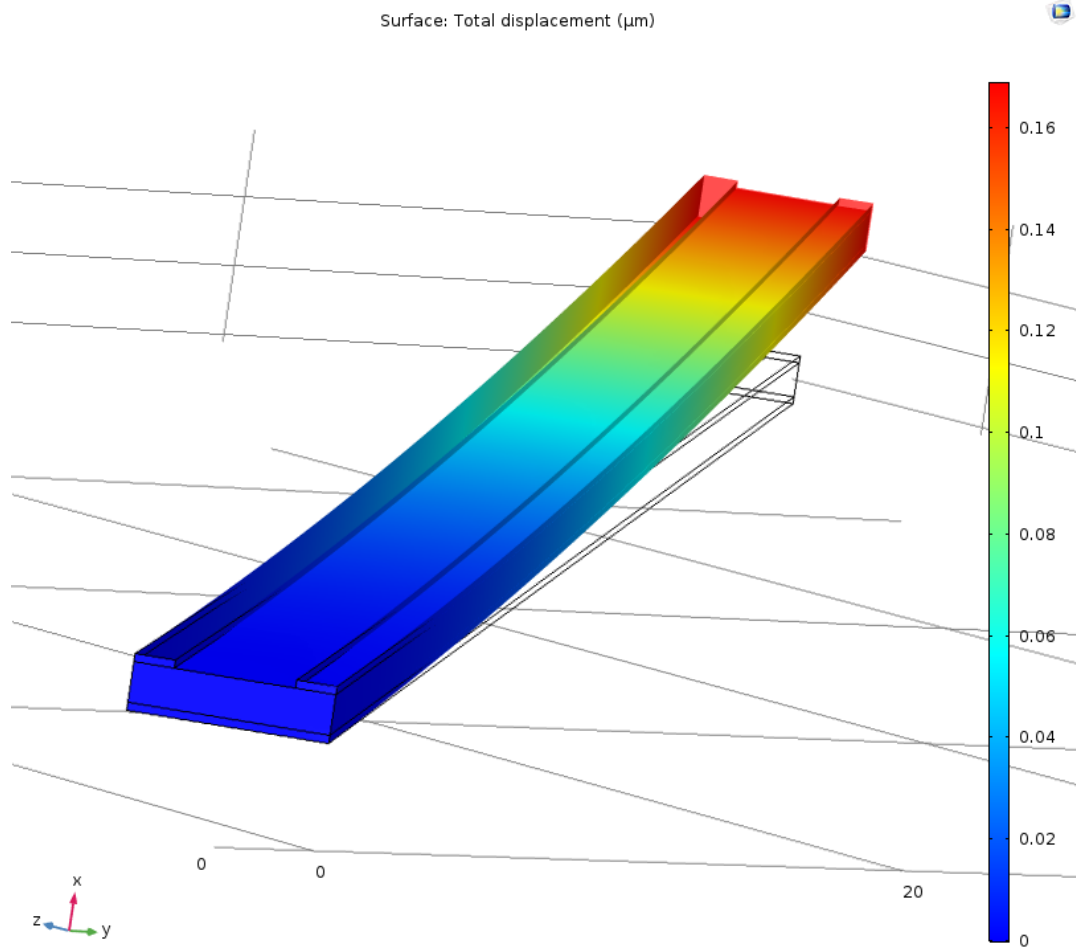


Figure 29. Displacement plot of single ground beam.

The simulation results for this design supports this analysis. The beam loses roughly half of its performance (though still compares favorably to aluminum nitride.) This is as expected, since the driving electric field differential has also been reduced by the same proportion: Instead of a lateral, top-surface electric field opposing an equal but opposite bottom-surface field, it now opposes a zero lateral field. Interestingly, the revised configuration has also reduced the torsional response, likely due to the reduction in the z-component of the electric field.

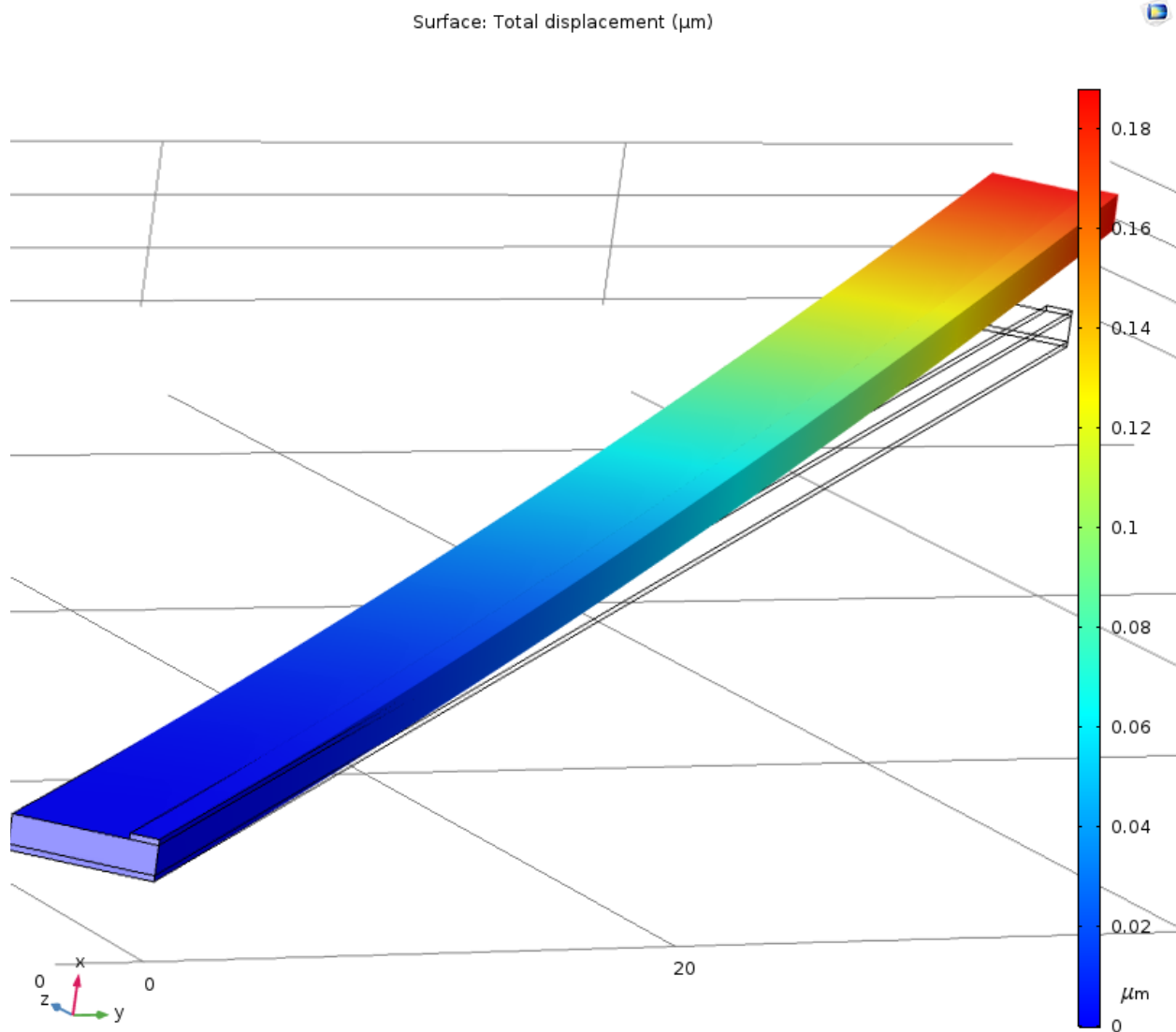


Figure 30. Revised electrode pattern with single top electrode, continuous bottom ground.

Simulations were also run with the top ground electrode removed. This modification would enable more versatility in incorporating this unimorph beam into more complex devices. More specifically, fabricating the reversing-polarity structure previously discussed (in which half of the beam bends upwards while the other half bends downwards, resulting in vertical deflection without tilt at the end of the beam) would be impracticable using existing monolithic fabrication

techniques. A design using only a single signal electrode could effect a polarity reversal without having somehow to cross-over two different electrodes. Surprisingly, removal of the second ground electrode on the top surface of the beam improved performance. This may be due to the increased vertical electric field component near the sidewall; this component may be driving a shearing strain response that augments the vertical deflection of the beam.

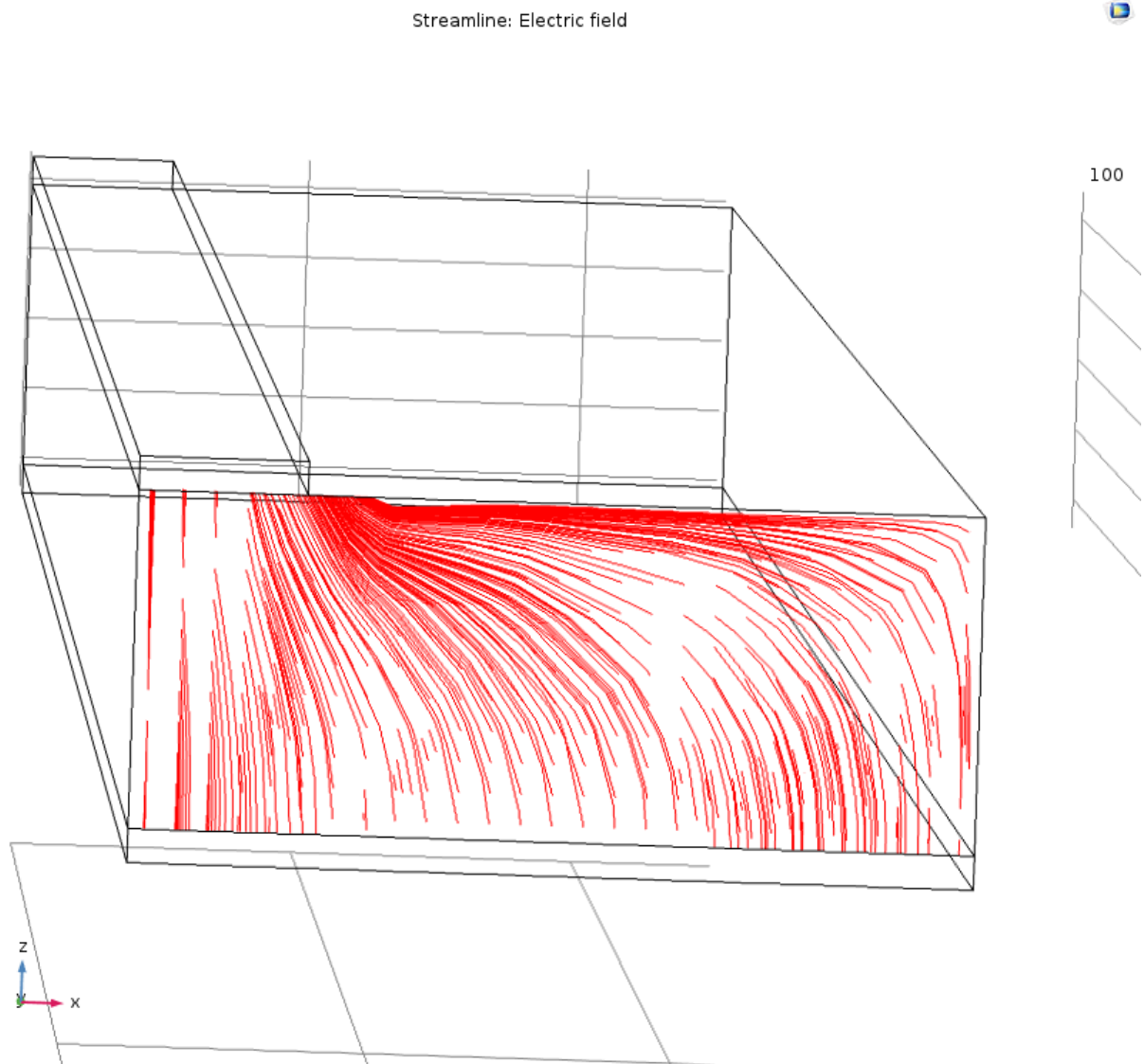


Figure 31. Streamline plot of unimorph beam with single top signal electrode and continuous bottom ground electrode.

Multistage Actuator

Taking advantage of these two distinct actuation mechanisms, and exploiting the flexibility permitted by the simplified electrode pattern, it is possible to fabricate devices that take advantage of one or both mechanisms within a single device layer, and to build upon their individual displacements to achieve larger out-of-plane displacements than what is currently possible in piezoelectric devices. The so-called “folded” bimorph design published as part of a variable capacitor design represented a simple multi-stage device. Using two separate bimorph beams, with the second beam anchored to the deflecting end of the first beam, it was able to both cancel out the tilting introduced by the bending beam, while also increasing the effective length of the bending beams without increasing the largest dimension of the device footprint. That published design had several limitations. First, the hysteresis among the various sputtered metal and aluminum nitride layers resulted in substantial built in stresses—this resulted in a substantial upward curve in the beam upon release, even at zero applied electric field. Second, none of the bimorph beam components incorporated a polarity change. As a result, when the first beam deflected upwards, it increased the existing tilt, causing the second stage to angle downwards even further. The upward bending of the second-stage beam still resulted in a net upward deflection of the capacitor, but this deflection could have been substantially higher without the built-in bending. Moreover, the publication showed prototypes that were unnecessarily bulky with respect to their performance. While the actuation moved the capacitor plate up to 8 micrometers above the pre-release device plane, upon release the beam-beam interface would rise up to 80 micrometers. This creates substantial challenges in integrating and packaging the device.

As discussed, lithium niobate does not share the same susceptibility to hysteresis, while the reduction in the total number of layers reduces the likelihood of built-in stresses due to thermal mismatch. This makes it easier to avoid the problem of zero-bias bending. Moreover, the use of the reverse-polarity beam design—enabled by the single top-electrode pattern—allows each stage to contribute to the total vertical deflection without introducing detrimental tilting.

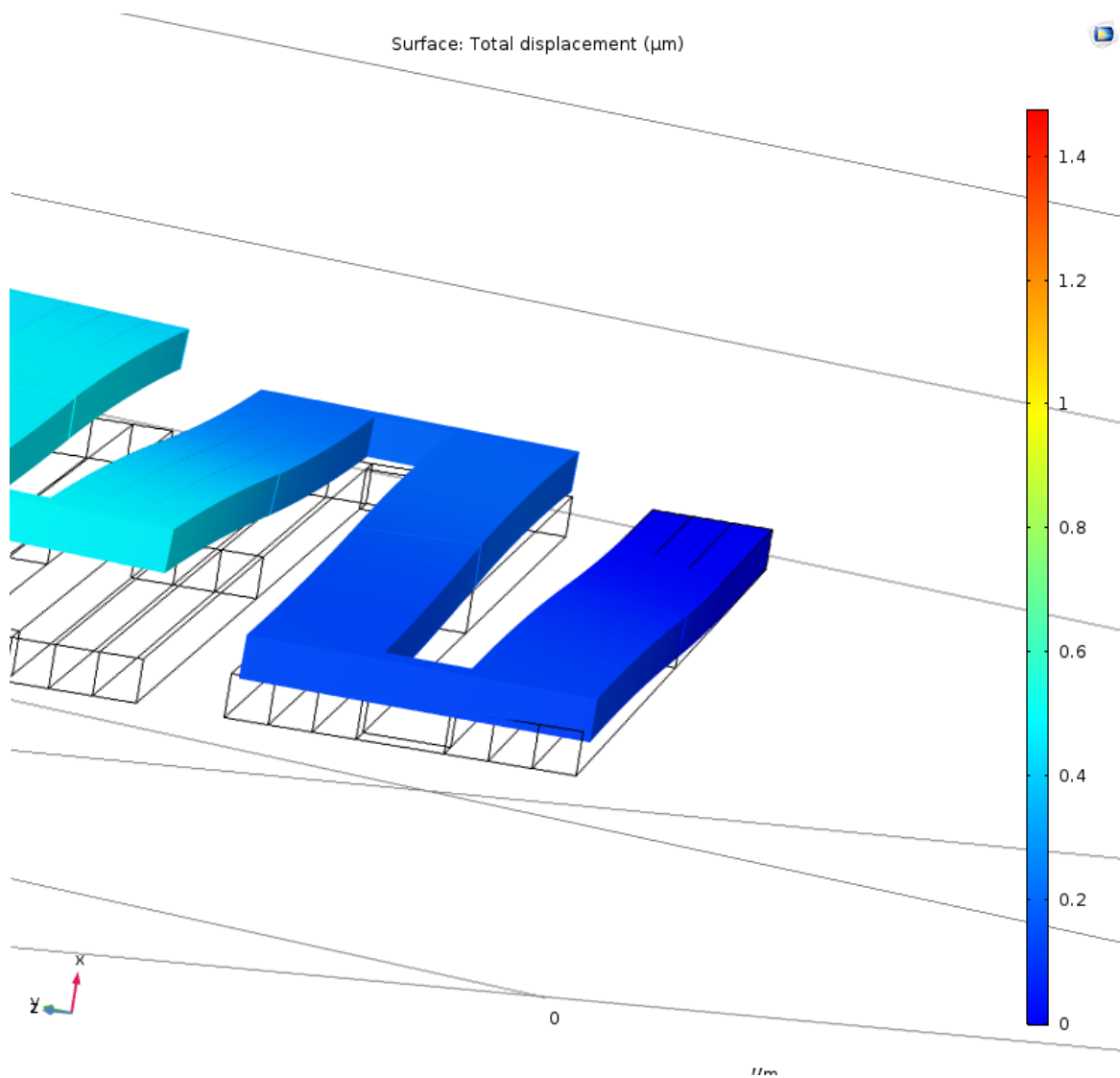


Figure 32. Multiple bending beams in stages provide greater total displacements.

To design an optimized, multistage device, the first step is to optimize the component structures: each individual bending and torsional beam. First, the parametric sweep functions in COMSOL were used to tune the dimensions of the simple actuator beams, within the constraints of the device requirements and practical microfabrication limits. Up to a limit, thinner lithium niobate layers produced superior bending due to the cross-sectional area and stiffness. With prototype fabrication in mind, various vendors were explored; this search yielded a source that could produce a one-micrometer thick lithium niobate layer bonded to metal on substrate. This constraint was thus used for optimization. Tolerances of fabrication processes available on campus allow single micron resolution at best, a preferred minimum feature size of 2 micrometers. This provided further constraints. For equal thickness and a constant top electrode coverage as a fraction of total beam width, increasing the width of the beam would generally reduce the amount of deflection as the beam stiffness increased. Thus, in order to optimize the design, it makes sense to reduce the width of the beam within the limit of other design constraints. For multistage designs, a reduced beam width would also permit more stages of the device to fit within the same device footprint, in turn improving the performance of the design as a whole.

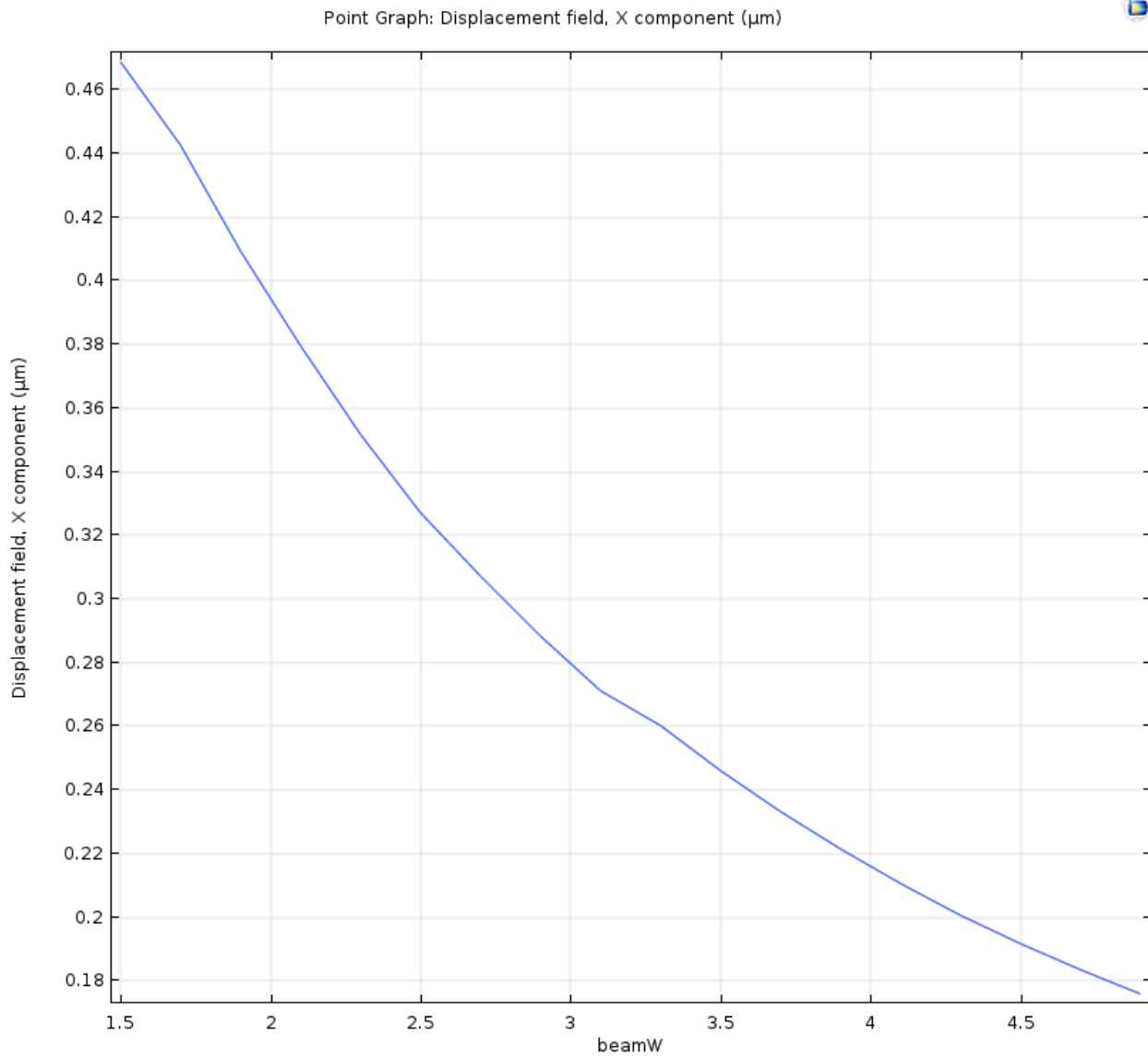


Figure 33. Parametric plot of vertical deflection of a single, 100 micrometer unimorph beam as a function of beam width.

Tuning the beam width and electrode width demonstrated an optimum electrode coverage fraction that would maximize deflection for a given piezoelectric beam width. For wider piezoelectric beam widths, this fraction shifted slightly. For a 3-micrometer wide beams, this optimal fraction is very nearly one-third, or one-micrometer wide electrodes. As the aforementioned considerations dictated a narrower beam, this value was selected as a round

number that would likely be optimized with an electrode size that conforms to the minimum feature size.

Next, the individual components were assembled into multistage designs. Throughout the design process, it was observed that the non-uniform electric field intrinsic to this design would continue to produce unwanted strain components. In the more complex devices, these unwanted components would often add up and undermine performance of the device. One of the most successful designs exploited both the bending unimorph beams and the torsional beams. Moreover, it relied on the symmetry of the lithium niobate crystalline structure to cancel out many of the undesirable strain components.

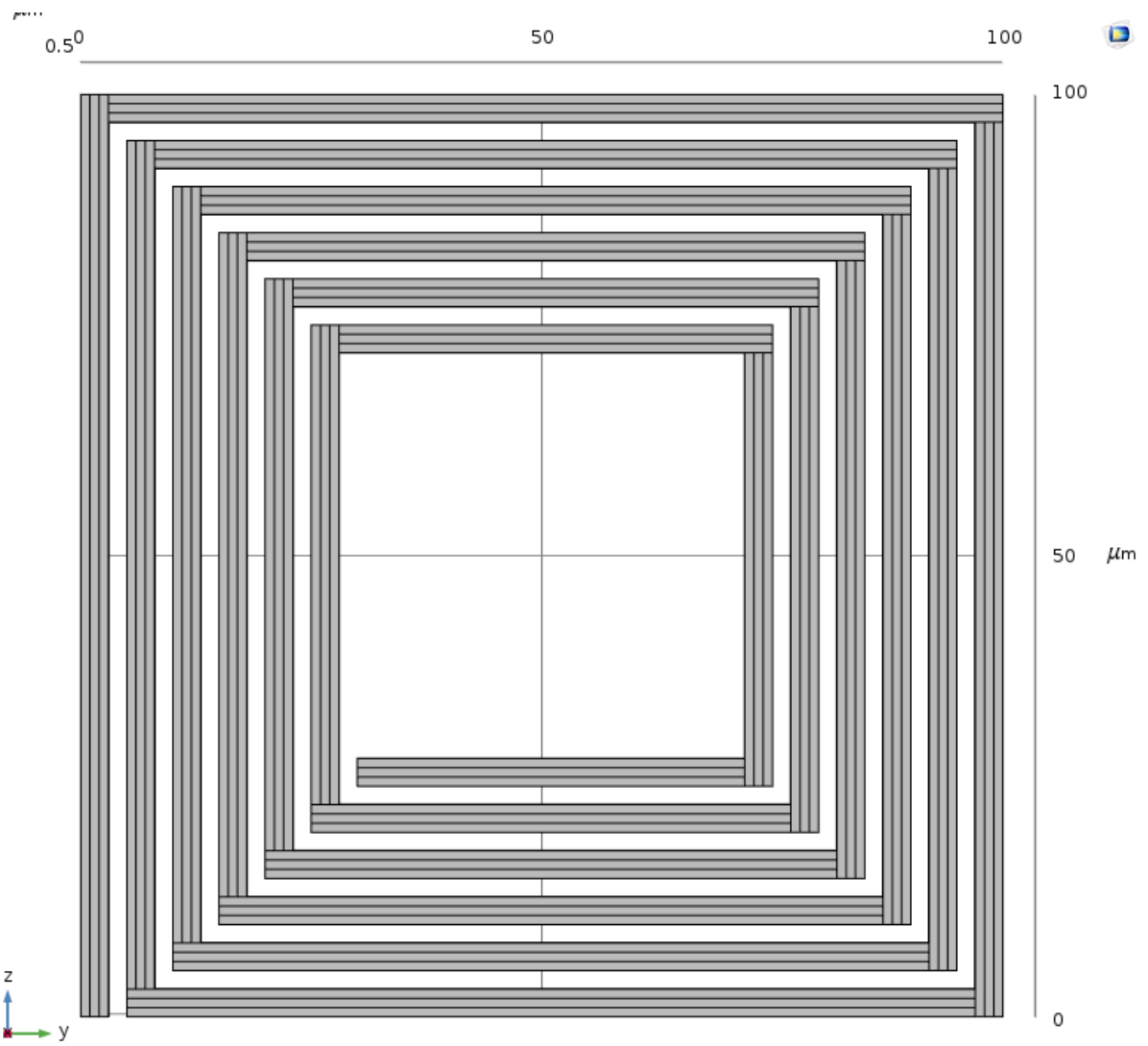


Figure 34. Layout of spiral actuator design.

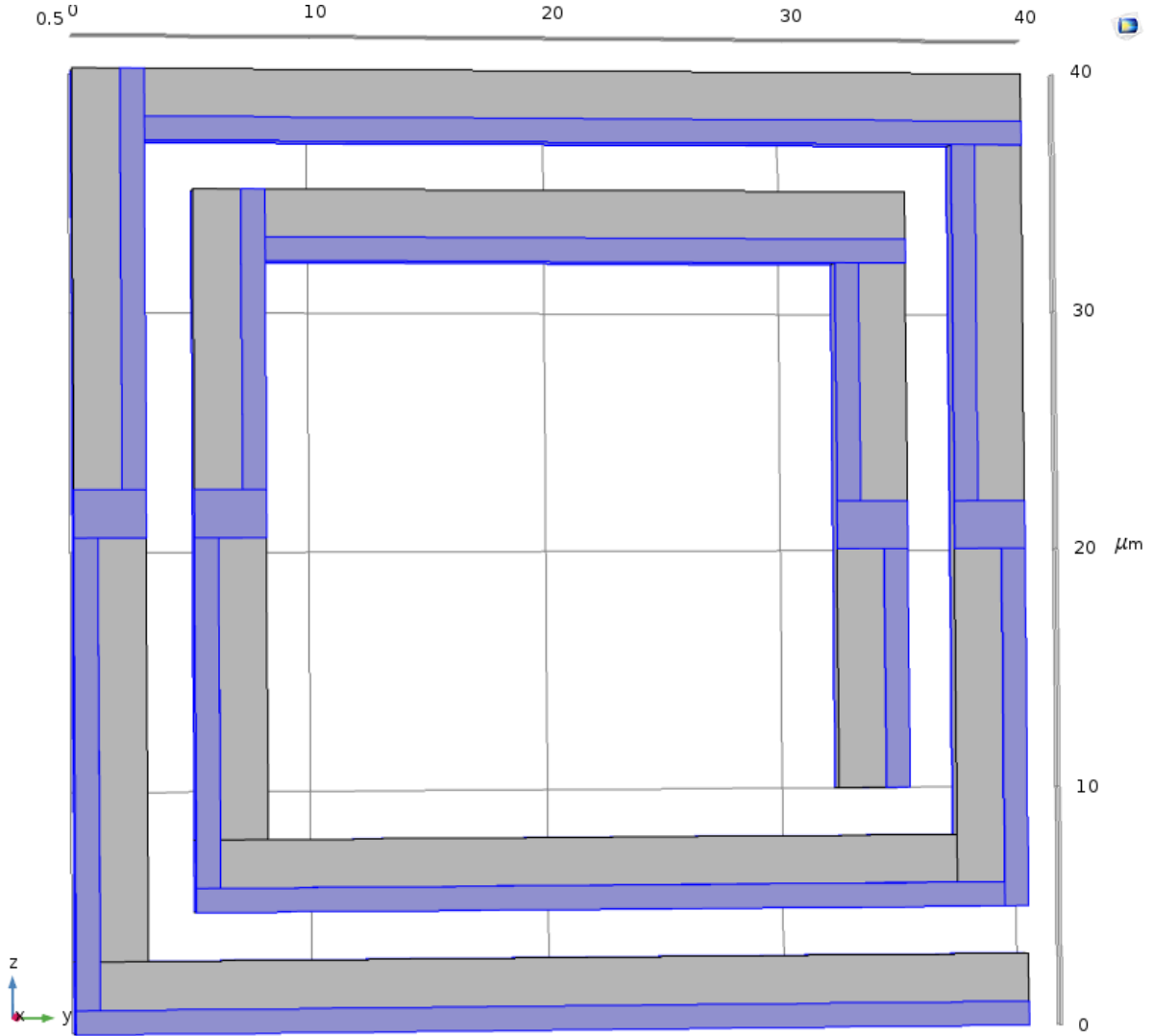


Figure 35. Simplified and scaled layout of spiral design to show top electrode pattern.

The crystallographic orientation of the device in the COMSOL simulation was achieved using two separate steps. The device model was constructed to be oriented in the X-cut, with the device components laid out in the YZ plane of the primary coordinate system for the simulation. This is reflected in the preceding figures, where the x-axis is normal to the plane of the document. The second step reflects the in-plane rotation of the device about the z-axis of the wafer (the x-axis of the crystallographic structure of the lithium niobate.) This can be achieved

by either using a transformation to rotate the structure about the x-axis in the primary coordinate system, or using a secondary coordinate system for the piezoelectric multiphysics simulation. In COMSOL, using a rotated coordinate system in order to keep each beam component aligned with the primary coordinate system provides substantial benefits, particularly in post-processing, but substantially complicates parametric sweeps of orientations.

In the preceding figures, a rotated coordinate system was used. Beams aligned with the y-axis in the figures are in fact rotated 40° off the z-axis in the x-cut plane; they exhibit primarily torsional actuation, and the single-polarity electrode pattern results in a continually increasing tilting angle moving away from the anchored end of the beam. This tilt causes the next perpendicular beam to tilt, causing the far end of that beam to rise. Moreover, beams along this in-plane orientation exhibit substantial bending, and the reversing-polarity electrode pattern causes the S-shaped bending pattern that contributes to upward deflection without introducing an increasing curve along the beam. The end of this beam connects perpendicularly to the third stage, another torsional beam. Because this beam-beam interface already rests at an angle relative to the plane of the device, the next torsional beam does not introduce an upward deflection—instead, it largely cancels out the tilt introduced by the first beam. As a result, the fourth beam—another bending beam—is nearly parallel to the device plane, and introduces further deflection. This pattern can be repeated within the limit of the device footprint.

The demonstrated design consists of six sets of four beams. The actuation signal is a DC signal of 10 volts. This value was selected to be within the range of MEMS devices in similar devices—typical publications demonstrate actuation voltages ranging from several volts to over 50 volts, depending on applications. Another consideration was the dielectric breakdown point of

lithium niobate. The selected voltage should not cause the electric field in the lithium niobate to exceed the breakdown field strength in any of the currently proposed designs. This voltage yielded a total vertical displacement of over 12 micrometers.

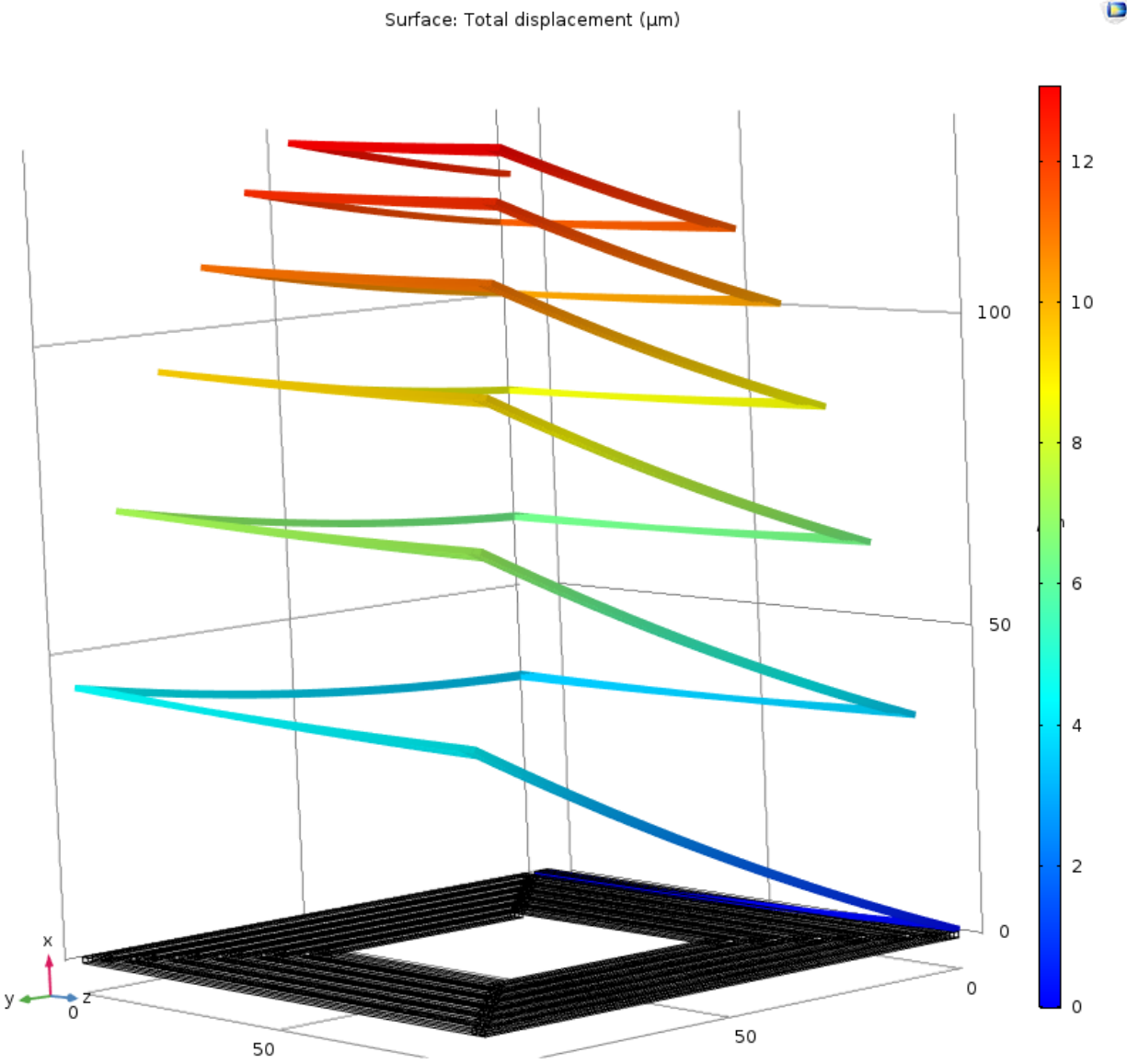


Figure 36. Simulation of spiral actuator design.

CHAPTER SEVEN: RESULTS AND CONCLUSIONS

Results

The novel electrode pattern presented in this paper enabled the design of a unimorph piezoelectric bending actuator, one that consistently outperformed a traditional bimorph actuator of comparable dimensions and tolerances. Additionally, this electrode pattern led to the design of a novel torsional actuator beam. Additionally, the flexibility of this design and ability to fabricate both simple actuators in the same piezoelectric layer has permitted the design of novel, multistage actuators. The spiral actuator achieves a simulated vertical displacement of over 12 micrometers within a footprint of 100 by 100 micrometers. In contrast, a multistage actuator comprised of aluminum nitride bimorph beams achieves displacements on the order of a single micrometer within the same footprint.

Comparison to Published Works

Individual cantilever components were designed using similar constraints as devices and designs published in existing literature. The publication of the variable capacitor disclosed modeled results of 1.3 micrometer deflection from a single, 200 micrometer aluminum nitride cantilever actuated with 5 volts. [2] The present design produces a model of equal length and slightly lower thickness that can yield deflection of 450 nanometers.

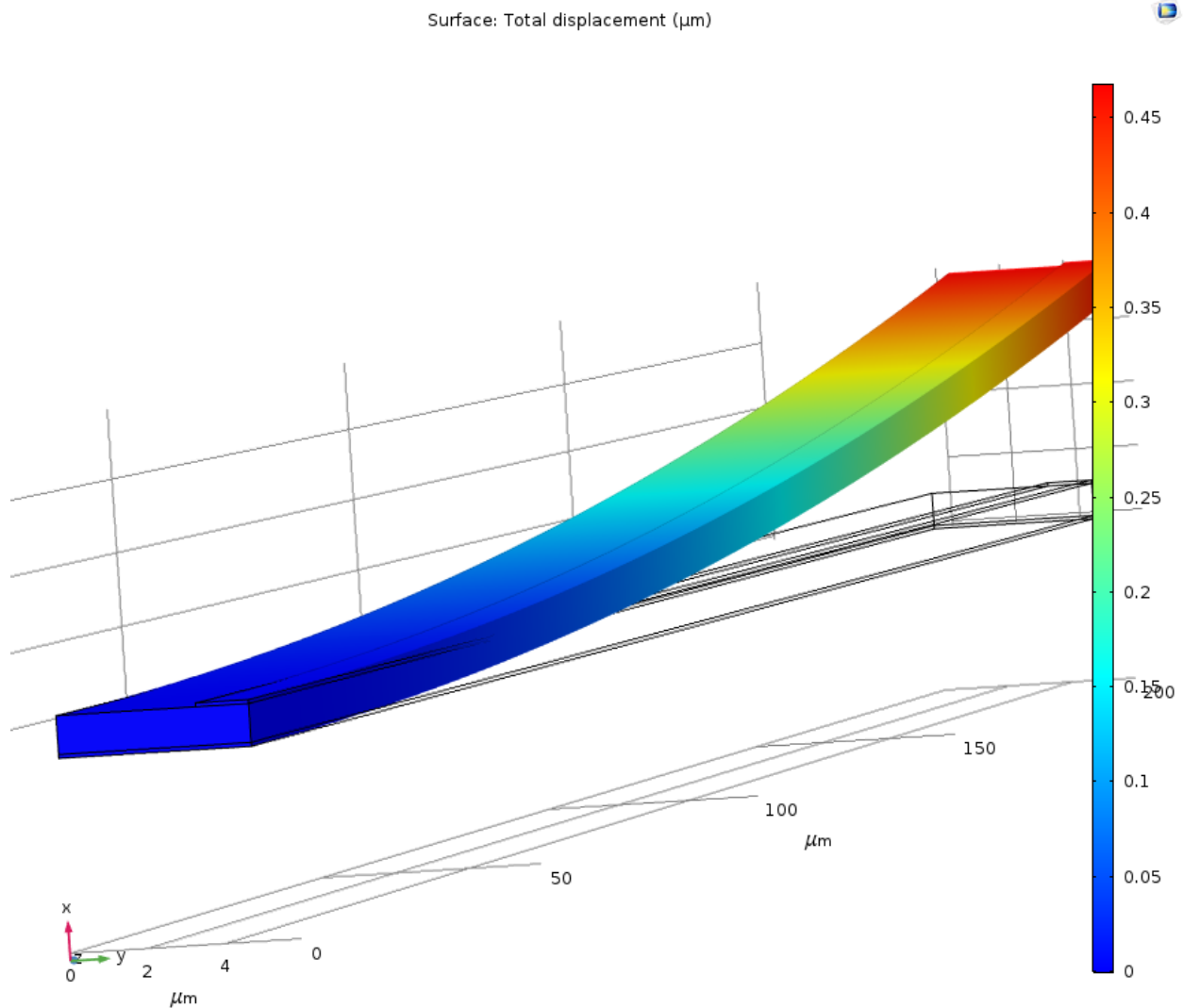


Figure 37. Simulation of 200 micrometer cantilever beam.

An exact comparison is challenging because the precise bending moment depends in part on the width of the beam, a value not specified in the paper. A COMSOL simulation of the basic cantilever bimorph modeled in that paper (with a width of 5 micrometers selected to match the lithium niobate unimorph beam) yielded less favorable results. The most likely cause of the discrepancy is the selection of a different width.

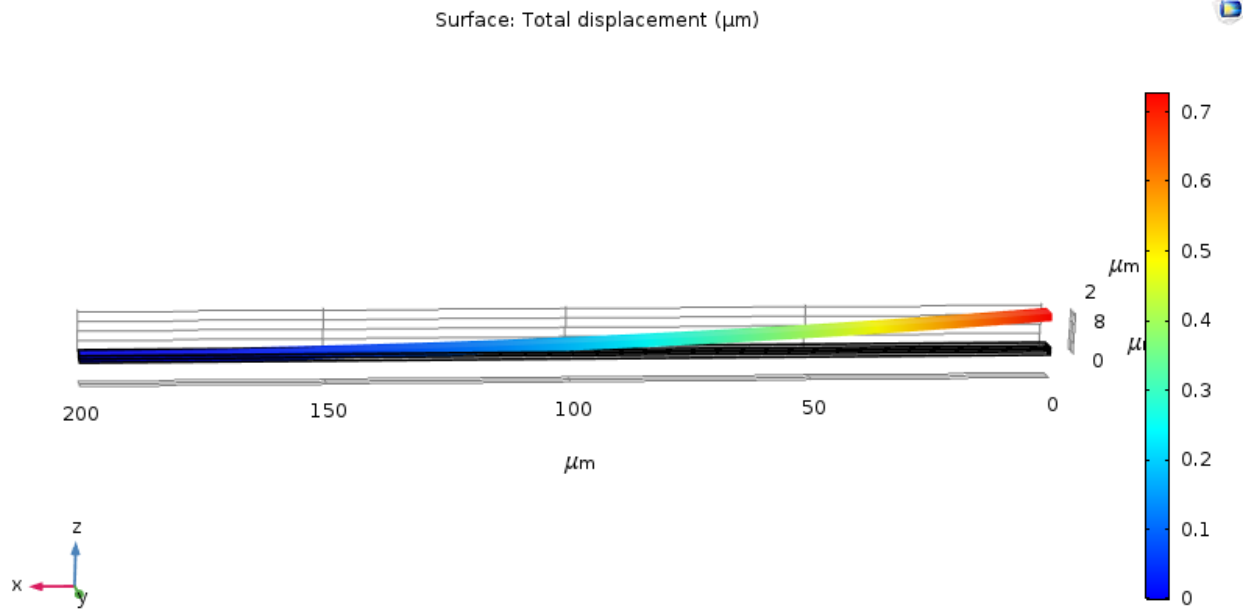


Figure 38. COMSOL simulation of bimorph modeled by Kawakubo et al.

Comparing beams of equal piezoelectric layer thickness, rather than equal total beam thickness, yields more favorable simulation results for the unimorph design. Altering only the thickness of the lithium niobate layer to match the 500 nanometer thickness of the aluminum nitride layers yields deflections of roughly 750 nanometers, exceeding the deflection of the simulated aluminum nitride bimorph.

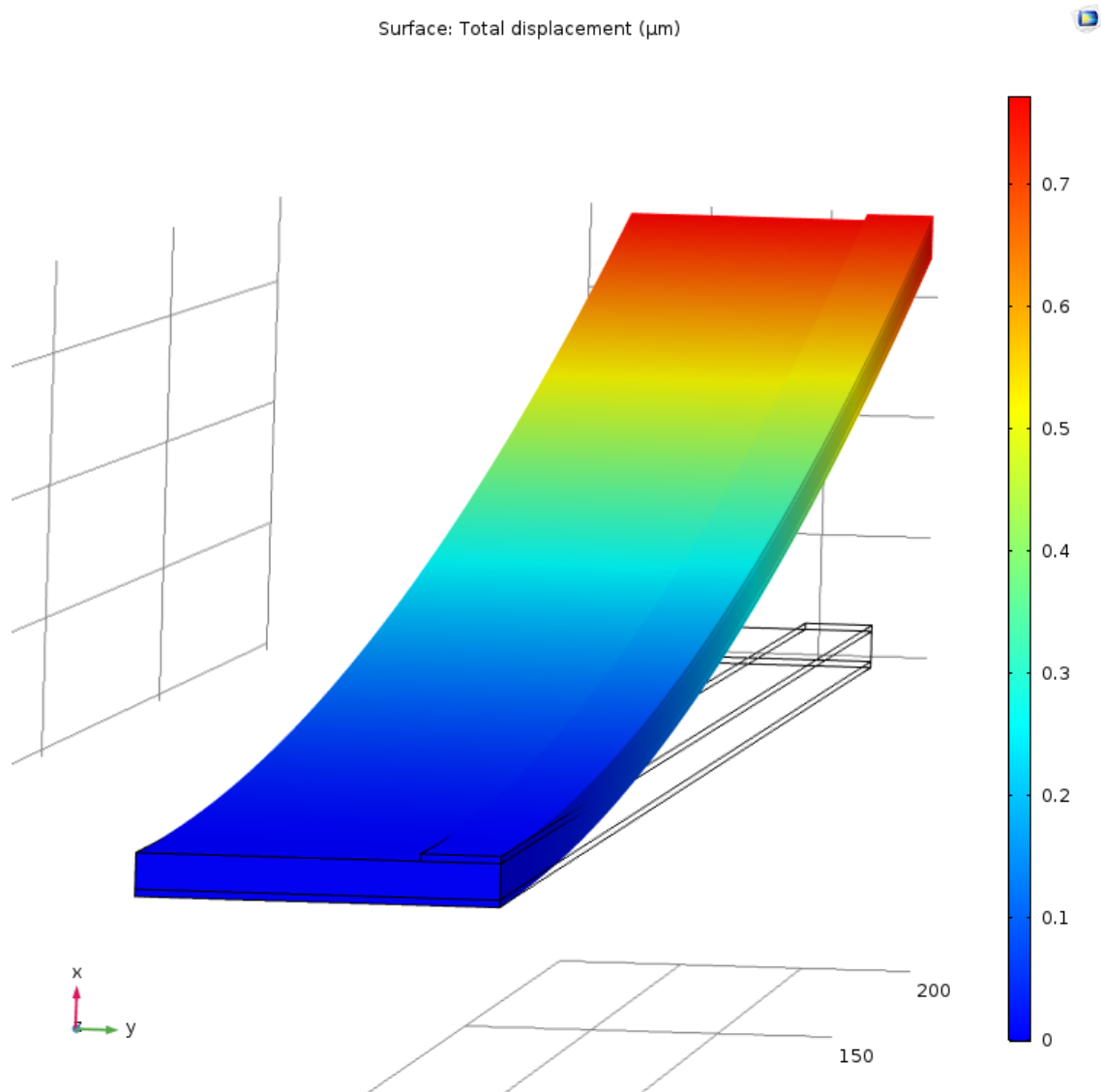


Figure 39. Simulation of half-micrometer thick unimorph beam.

Using single-polarity unimorph beams in the same folded design presented by the paper yielded actuation point displacements of 900 micrometers for a one-micrometer thick lithium niobate layer. This falls within the range of reported deflections for various aluminum nitride devices using varying configurations (reported deflections ranging from close to zero vertical actual to two micrometers.) [2] The results from both the present study and Kawakubo paper compare favorably to results published Mahameed, who disclosed an aluminum nitride bimorph

with one active and one passive piezoelectric layer, yielding deflections of 650 nanometers or less from their various designs in simulation. [1]

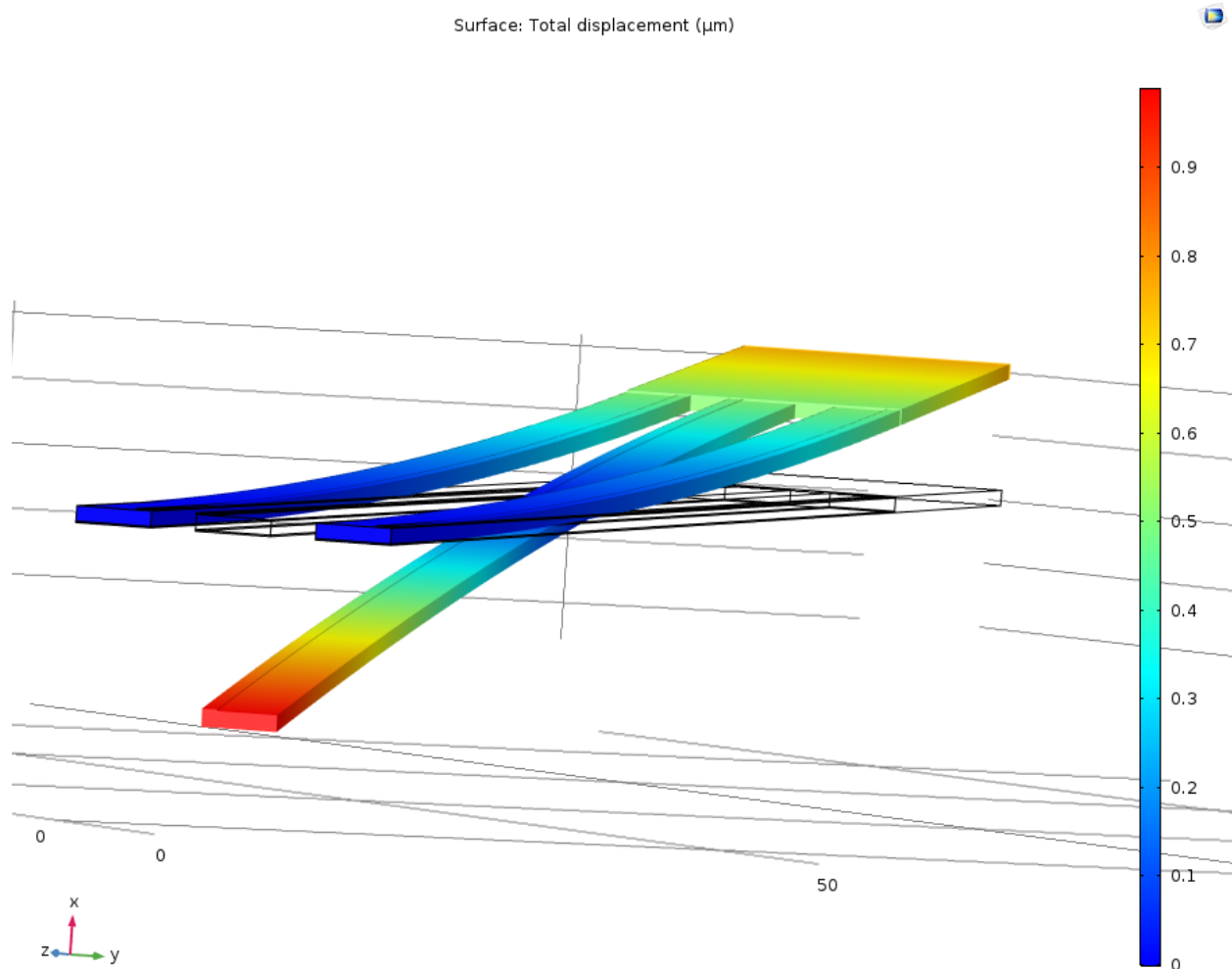


Figure 40. Folded capacitor tuning actuator using unimorph beam components (1 micrometer thick).

One advantage of the unimorph beam design is the ability to change polarity without the use of complex metallization and via holes. This enables greater flexibility in modifying the multistage actuator, as in the following modified design using polarity reversals along each beam. Using similar specifications, this design yielded vertical displacements of 500 nanometers in simulations. While this is lower than the previous unimorph-beam based design, and below the

average of reported results from the published study, this tradeoff comes with noteworthy benefits. The actuating beam remains parallel to the substrate near the actuation point, which is the highest moving point on the beam. Unlike aluminum nitride design, in which the folding point linking the three beams rose up to 80 micrometers from the pre-release elevation (and generally remained around an order of magnitude higher than the desired displacement at the actuation point) this design minimizes unwanted movement and bulkiness. [2] Whereas the previously published design may present serious challenges to integration with other components, this design may be packaged more closely with other components without risk of making contact.

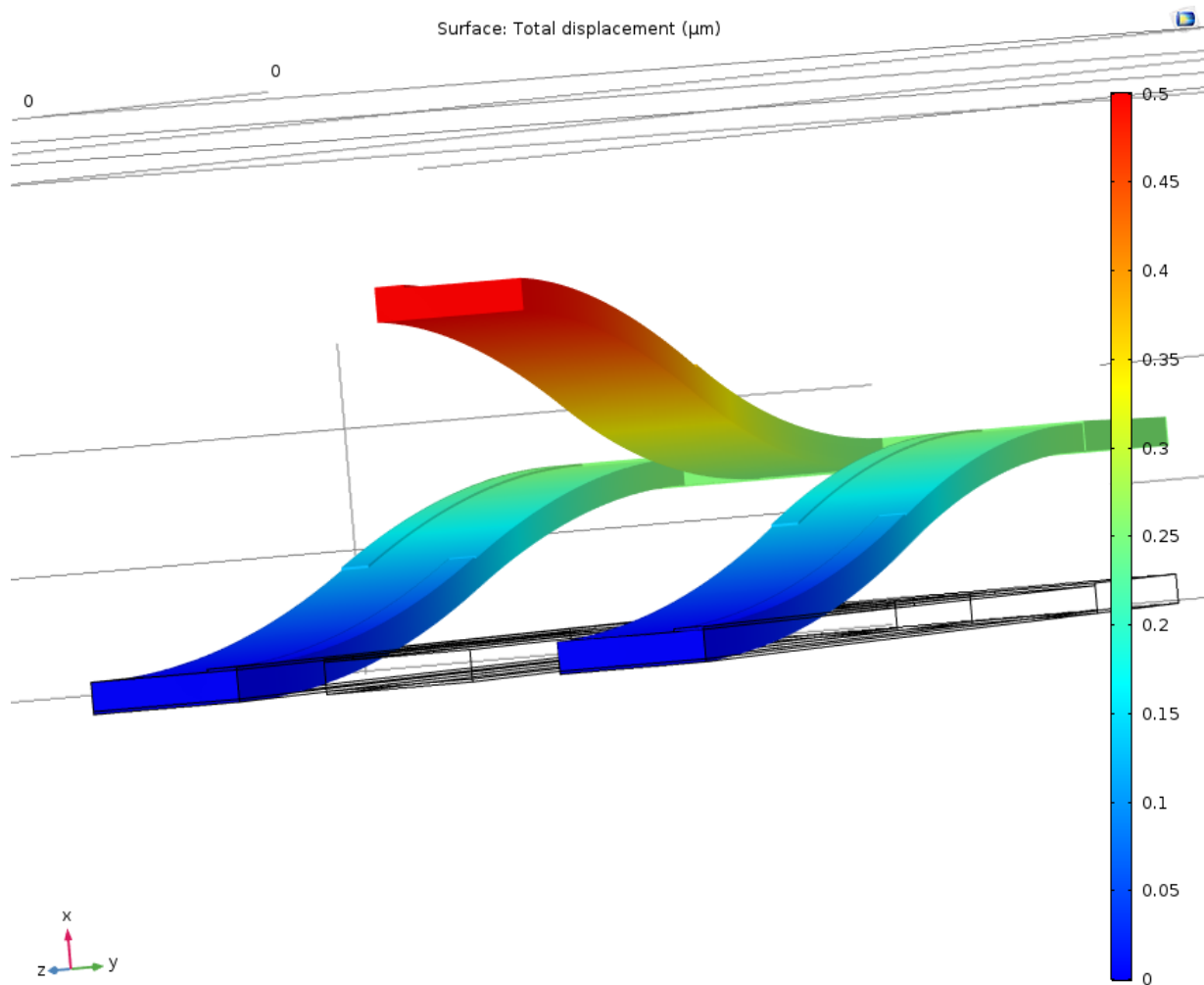


Figure 41. Folded capacitor tuning actuator using dual-polarity unimorph beam components (1 micrometer thick).

The current designs do not outperform the published results for PZT bimorph actuators. However, because lithium niobate shares the compatibility advantage of aluminum nitride, it would be a preferred choice over a PZT devices in most applications, despite the lower displacements—much as aluminum nitride has been. A 1000 micrometer long unimorph beam using the present design yielded just over 25 micrometers of deflection in response to a 10 volt signal. While this slightly exceeds the performance of an aluminum nitride bimorph of similar dimensions, it falls far short of the reported 80 micrometers and 280 micrometers yielded by the

two PZT actuators. The superior performance of the PZT should not be surprising; the cited study calculated a d_{31} of -92 picocoulombs per newton. [3] This far exceeds the reported d_{31} of aluminum nitride, only -2.65 picocoulombs per newton. PZT also compares favorably to the analogous metric for lithium niobate. Recall that the unimorph design relies on d_{21} , the coupling between the lateral tangential electric field component of the electric field and the mechanical strain in the longitudinal direction. Thus, it is proper to compare the strain coefficient of PZT to the effective d_{21} for the orientation of the lithium niobate beam (40° in-plane, off X-cut.) This value is only 22 picocoulombs per newton. The drastic difference in performance is due to the difference in electric field strength for both devices. While a traditional bimorph structure with a 10 volt DC signal would produce uniform electric fields on the order of 5 megavolts per meter, the innovative electrode electrode pattern in a unimorph beam produces tangential electric field components that are orders of magnitude smaller.

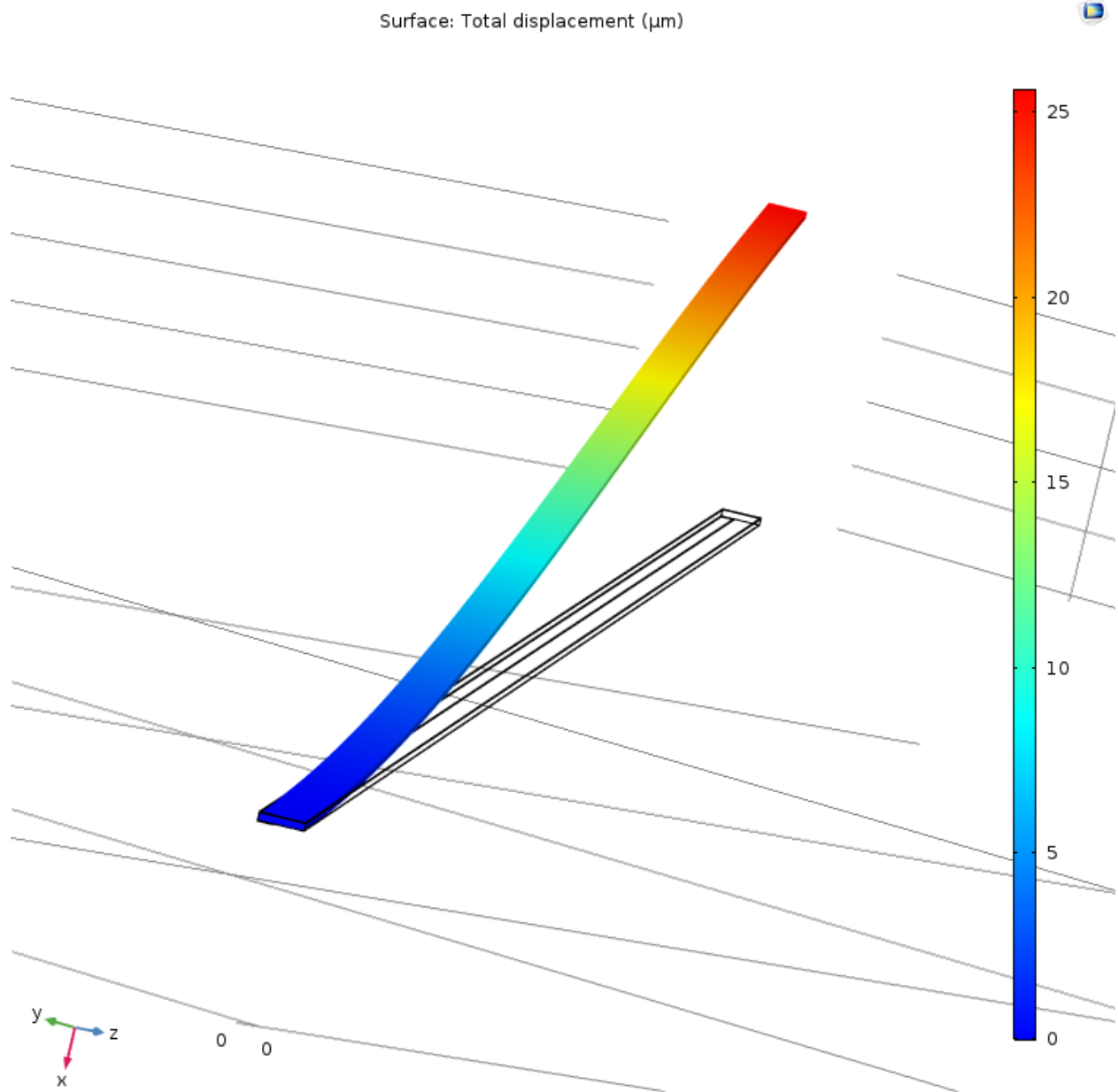


Figure 42. COMSOL simulation of 1000 micrometer unimorph beam.

Conclusions

This novel design yields substantial advantages over existing piezoelectric actuators in both cost and performance. The simplified design and fabrication process means that this novel design could yield actuators that are less expensive and more robust than existing piezoelectric

actuators. The maximum deflection of individual unimorph beams is roughly comparable to existing process-compatible piezoelectric bimorphs of similar dimensions. However, due to the ability to use the flexible conductor pattern to build complex, multi-beam devices that take advantage of in-plane anisotropy, this design methodology can yield superior displacements compared to multistage bimorph actuators in a similar footprint.

Such actuators are already used extensively in such applications as energy harvesters and inertial sensors—demonstrating that the market already favors piezoelectric transduction, despite its limitations. This new design could readily supplant these existing actuators. Moreover, the improvements in displacement helps to mitigate the chief limitation of piezoelectric devices: their low displacement compared to other actuation methods. Because this design substantially increases the movement achieved within the same device footprint, using comparable applied voltages, it can reduce the threshold voltage or power consumption of existing MEMS components or even enable novel applications that require the superior displacement resolution provided by piezoelectric actuators but higher maximum displacement than current piezoelectric devices.

Work has already begun on the next step in this research: Fabricating a prototype of these designs. A full microfabrication process for these devices has already been designed. While actual devices do not always match the performance predicted by models, finite element simulation has already proven to be a powerful predictive tool. Moreover, the performance of these simulated designs are such a substantial improvement over existing devices that even if the simulation results prove to be inaccurate or overly optimistic, development of this area of research seems worthwhile.

LIST OF REFERENCES

- [1] R. Mahameed, N. Sinha, M. B. Pisani, and G. Piazza, "Dual-beam actuation of piezoelectric AlN RF MEMS switches monolithically integrated with AlN contour-mode resonators," *Journal of Micromechanics and Microengineering*. Vol. 18, No. 105011, Sept 2008. [Online]. Available: <http://stacks.iop.org/JMM/18/105011> [Accessed July 2019].
- [2] T. Kawakubo, T. Nagano, M. Nishigaki, K. Abe, and K. Itaya, "RF-MEMS Tunable Capacitor With 3 V Operation Using Folded Beam Piezoelectric Bimorph Actuator," *Journal of Microelectromechanical Systems*. Vol. 15, No. 6, pp. 1759-1765, Dec 2006. [Online] Available: <https://ieeexplore.ieee.org/abstract/document/4020273> [Accessed July 2019].
- [3] M. Hoffmann, T. Leuerer, R. Liedtke, U. Bottger, W. Mokwa, R. Waser, "Integration of Piezoelectric PZT Thin Films with Internal Electrodes into an Actuator Structure for MEMS Applications," *Integrated Ferroelectrics*. Vol. 50, No. 1, pp. 21-32, Oct 2002.
- [4] S. O. Reza Moheimani and A. J. Flemming, "Fundamentals of Piezoelectricity," in *Piezoelectric Transducers for Vibration Control and Damping*. London: Springer-Verlag, 2006, pp. 9-35.
- [5] B. A. Auld, *Acoustic Fields and Waves in Solids, Volume I*. Malabar, FL: Robert E. Krieger Publishing Company, 1990.
- [6] A. C. Fischer, F. Forsberg, M. Lapisa, S. J. Bleiker, G. Stemme, N. Roxhed, and F. Niklaus, "Integrating MEMS and ICs," *Microsystems & Nanoengineering*. Vol. 1, 15005, May 2015. [Online]. Available: <https://doi.org/10.1038/micronano.2015.5> [Accessed May 2019].
- [7] S. Trolier-McKinstry, and P. Muralt, "Thin Film Piezoelectrics for MEMS," *Journal of Electroceramics*. Vol. 12, Issue 1-2, pp. 7-17, Jan 2004. [Online]. Available: <https://link.springer.com/article/10.1023/B:JECR.0000033998.72845.51> [Accessed May 2019].
- [8] "Standards on Piezoelectric Crystals, 1949" *Proceedings of the I.R.E.* December 1949
- [9] *IEEE Standard on Piezoelectricity*, ANSI/IEEE Standard, 176, 1987.
- [10] R. T. Smith and F. S. Welsh, "Temperature Dependence of the Elastic, Piezoelectric, and Dielectric Constants of Lithium Tantalate and Lithium Niobate," *Journal of Applied Physics*. Vol. 42, No. 2219, 1971. [Online]. Available: <https://aip.scitation.org/doi/10.1063/1.1660528> [Accessed May 2019].
- [11] V. Ya. Shur, I. S. Baturin, E. A. Mingaliev, D. V. Zorikhin, A. R. Udalov. And E. D. Greshnyakov, "Hysteresis-free high-temperature precise bimorph actuators produced by

direct bonding of lithium niobate wafers,” *Applied Physics Letters*. Vol. 106, 053116, Feb 2015. [Online]. Available: <https://aip.scitation.org/doi/abs/10.1063/1.4907679> [Accessed January 2019].

- [12] Wang Yue and Jiang Yi-Jian, “Crystal orientation dependence of piezoelectric properties in LiNbO_3 and LiTaO_3 ,” *Optical Materials*. Vol. 23, No. 1-2, pp. 403-408, Aug-Sept 2003. [Online]. Available: [https://doi.org/10.1016/S0925-3467\(02\)00328-2](https://doi.org/10.1016/S0925-3467(02)00328-2) [Accessed March 2019].